



Numerical reconstruction of a rapidly developing bow echo over northeastern Poland on 21 August 2007 using near-grid-scale stochastic convection initiation

Damian K. Wójcik^{1,2}, Michał Z. Ziemiański², Wojciech W. Grabowski³

5

¹Department of Atmospheric and Cryospheric Sciences, University of Innsbruck, Innsbruck, Austria

²Institute of Meteorology and Water Management - National Research Institute, Warsaw, Poland

³NSF National Center for Atmospheric Research, Boulder, Colorado

Correspondence to: Damian K. Wójcik, damian.wojcik@uibk.ac.at, damian.wojcik@imgw.pl

10 **Abstract.** A rapidly developing fast propagating meso- β -scale severe bow echo that developed over northeastern Poland on 21 August 2007 caused significant property damage and resulted in 12 fatalities. The operational model of Consortium for Small Scale Modeling (COSMO) with a horizontal grid spacing of 2.2 km is used for its numerical reconstruction but encounters significant problems despite favorable environmental conditions. Implementation of a new stochastic convection initiation scheme within a 9-member ensemble allows to
15 reconstruct the event as the cold-pool-driven convective system with maximum gusts close to the observed ones. The scheme uses small-scale temperature perturbations arguably resembling grid-scale convective boundary layer thermals that influence not only MCAPE and MCIN, but also the lower-tropospheric vertical shear. Initial and boundary conditions for the experiment are based on ERA5 reanalysis. Additional data assimilation of local surface observations improves the reconstruction of atmospheric environmental conditions. A supplementary
20 experiment tests the forecast sensitivity to an increase of low-to-mid tropospheric winds, and thus the vertical shear, and shows an increase of the maximum surface gusts within the ensemble when the convection initiation is implemented. The simulations' main drawbacks are about an hour delay in the development of maximum gusts and a tendency to produce isolated convective cells along the leading edge of the system's cold pool rather than a more coherent structure observed within the bow echo.

25 1 Introduction

Bow echoes (Fujita, 1978; Przybylinski, 1995) are a specific class of deep moist convection self-organization. They often produce high-impact weather, especially in the form of damaging winds and sometimes tornadoes (Fujita, 1978; Johns and Hirt, 1987; Gallus et al., 2008). However, bow echoes are especially difficult for numerical representation and prediction (Snively and Gallus, 2014; Lawson and Gallus, 2016). Bow echoes are
30 observed relatively frequently over the US (Klimowski et al., 2003), Europe (Pacey et al., 2021), and Poland (Celiński-Mysław and Palarz, 2017). As discussed in Klimowski et al. (2004), bow echoes may originate from a weakly organized group of cells, squall lines, or supercells. Their horizontal extent varies between 10 to 25 km for a single-cell bow to hundreds of kilometers for organized systems. Their lifespan varies from about 1 hour for the former to many hours for the latter (Klimowski et al., 2004). A special class of bow echoes is associated
35 with derecho events that feature the length of the damage swath of downburst clusters of several hundred kilometers (Johns and Hirt, 1987; Corfidi et al., 2016).



The idealized modeling studies indicate that bowing systems tend to form on the leading edge of convective cold pools in the presence of significant vertical wind shear (Weisman and Klemp, 1986; Weisman, 1992; 1993). A theory by Rotunno et al. (1988) (known as the RKW theory, see also a discussion in Bryan et al., 2006) explains the systems' organization and persistence via the approximate balance of the horizontal vorticity of the environmental flow and of the sufficiently strong cold pool flow at the pool's leading edge. The balance forces deep lifting and a formation of new convective cells at the leading edge, making bow echoes the cold-pool-driven (Coniglio et al., 2005) systems. Mature organized linear convection also tends to develop a mid-tropospheric inflow current, the rear inflow jet (RIJ), accelerated by the horizontal pressure gradient from condensational heating on the systems' leading edge (LeMone, 1983; Smull and Houze, 1987). Idealized modeling studies indicate an important role of RIJ for the bow echoes' persistence and the downward horizontal momentum transport (Weisman, 1992; 1993; Mahoney et al., 2009).

An ability of realistic numerical representation of such high-impact convective systems with contemporary convective-scale numerical weather prediction (NWP) models (Baldauf et al., 2011; Done et al., 2004; Saito, 2012; Yano et al., 2018) is important both for research and operational forecasting. Numerical models have already been used for successful numerical case studies of bow echoes developing over the US (e.g., Weisman et al., 2013; Xu et al., 2015; Parker et al., 2020; Liu et al., 2023), Europe (Toll et al., 2015; Mathias et al., 2017), and Poland (Taszarek et al., 2019; Figurski et al., 2021; Kolonko et al., 2023; Mazur and Duniec, 2023). However, such studies encounter several problems. Some stem from the inherent limited predictability of atmospheric processes at convective scales (Lorenz, 1969; Vallis, 2006; Palmer et al., 2014; see also a discussion in Lawson and Gallus, 2016). On the mesoscale, the predictability may be increased by a strong external forcing, for instance, by the underlying surface or by large-scale disturbances (Anthes et al., 1985). It is thus no surprise that the successful bow echo simulations concern mainly systems prone to increased predictability: relatively large or long-lasting (6 or more hours, including derechos), embedded within large convective systems, or developing under a significant external forcing (e.g., by fronts, Lawson and Gallus, 2016).

Other significant limitations stem from the models' uncertainties in representing grid- and sub-grid-scale processes (see extended discussions in Lawson and Gallus, 2016; and Varble et al., 2020). Bryan et al. (2003) and Lebo and Morrison (2015) show that the representation of deep convective updrafts requires at least 0.25 km horizontal grid spacing. Convective currents are therefore highly under-resolved in contemporary NWP models that typically feature horizontal grid spacing of O(1 km). The need to parameterize sub-grid processes introduces inevitable uncertainties as well. For instance, the representation of cloud microphysics significantly influences stratiform precipitation and convective updraft strength (e.g., Varble et al., 2014a; b). The overall impact of those model uncertainties on the simulated evolution of organized convective systems is still unclear (Varble et al., 2020).

The convective-scale simulation ensembles (e.g., Gebhardt et al., 2008; Clark et al., 2011; Hacker et al., 2011; Bouttier et al., 2012) aim to account for the forecast uncertainties. They typically apply perturbations to boundary and initial conditions (BC and IC, respectively) to account for large-scale uncertainties while the model ambiguities are represented by methods like stochastically perturbed parameterization tendencies (Buizza et al., 1999) or the stochastic kinetic energy backscatter (SKEB, Shutts, 2005). Such ensembles are also used for bow echo studies (e.g., Melhauser and Zhang, 2012; Lawson and Gallus, 2016; Grunzke and Evans, 2017; Lawson et al., 2020; Ribeiro et al., 2022), although they typically focus on long-lived systems.



From the process-level viewpoint, one of the main problems of convective-scale simulations is an insufficient representation of convection initiation (CI), especially for weak external forcings (Kühnlein et al., 2014; Clark et al., 2016; Hirt et al., 2019). To alleviate the problem, Hirt et al. (2019) and Puh et al. (2023) tested physically-based stochastic perturbations (PSP, Kober and Craig, 2016) of the temperature, vertical velocity, and humidity. Zeng et al. (2020) used the PSP and perturbations in the form of warm bubbles to account for the model errors in data assimilation, while Clark et al. (2021) used the scheme to represent boundary layer variability. The above studies (except a side-experiment by Clark et al., 2021) used perturbations of the horizontal scale of $O(10\text{ km})$ following the paradigm strongly advocated by Clark et al. (2021) of perturbation sizes of at least the model's effective resolution size (Skamarock, 2004).

We propose and apply a stochastic CI scheme, new in the context of convective-scale NWP applications, that contravenes the paradigm and deliberately uses temperature perturbations of horizontal scale possibly close to $O(1\text{ km})$. Particularly, we conjecture that such perturbations are sufficient for the model moist dynamics to explicitly represent the upscale growth and organization of convection, despite the model's diffusive properties (see a discussion in Palmer, 2019). The $O(1\text{ km})$ perturbation scale has strong physical justification, being the scale of observed shallow convective updrafts interacting with the boundary layer (Marquis et al., 2021, and references therein; see also Grabowski, 2023). The scale also coincides with the scale of the contemporary NWP horizontal grid. We demonstrate that the scheme allows a contemporary convective-scale NWP model to represent a high-impact, rapidly developing, isolated bow echo of Orlanski's (1975) meso- β -scale as the cold-pool-driven convective system with maximum gusts close to the observed ones, as long as correct large-scale environmental conditions are used.

The study's object is an isolated bow echo that developed within a warm air mass over northeastern Poland on 21 August 2007 (Fig. 1) and caused substantial fatalities and damages. Our process-oriented strategy reproduces the large-scale atmospheric environment in a deterministic sense, applying available reanalysis and observations, and uses a 9-member ensemble, driven only by random representations of CI. The use of such a CI-oriented ensemble is new for bow echo studies but reminds Lawson et al. (2020) who used only SKEB perturbations. Standard COSMO (Consortium for Small Scale Modeling) NWP model (Baldauf et al., 2011) and ERA5 reanalyses (Hersbach et al., 2020) are used. An additional novelty is in augmenting the results of global ERA5 reanalysis with mesoscale data assimilation, using available surface observations. That follows operational procedures of augmenting global DA with regional DA for regional NWP (e.g., Baldauf et al.; 2011; Bučánek and Brožková, 2017; Müller et al., 2017). We use operational COSMO nudging (Schraff and Hess, 2021) for that purpose.

After analysis of the convective system's environmental conditions and development, we demonstrate that the standard convective-scale COSMO operational NWP model without the CI scheme has significant problems with forecasting the system even with realistic environmental conditions. After implementing the stochastic CI, we analyze its influence on the environmental conditions, including CAPE, CIN, and shear. Next, we analyze the dynamics of the developing convection, focusing on the cold-pool-driven mechanism and RIJ formation. An additional experiment investigates how a slight increase in low-to-mid tropospheric wind shear influences the dynamics of convective development. A comparison of the experiments' results with available observations allows to identify inevitable imperfections of the system's numerical representation.

The paper is organized as follows. Section 2 describes the pre-storm weather conditions and the development of the 21 August 2007 bow echo system. Section 3 presents the data and models used for the study. Section 4



discusses a reconstruction of the initial conditions for the prognostic experiments and Section 5 discusses the results of the experiment without the CI scheme. The results of experiments with CI are presented in Section 6. Additional simulations involving increased low-to-mid tropospheric wind shear are discussed in Section 7. Section 8 discusses the development of the RIJ in the forecast most closely resembling the actual system development. The paper ends with the summary and conclusions in Section 9.

2 The bow echo and its environmental conditions

During the early afternoon of 21 August 2007, an isolated bow echo developed rapidly over northeastern Poland. The system generated near-surface wind gusts reaching 35 m s^{-1} , caused substantial property damage on land and capsized tens of sailing boats. The system had an exceptionally strong social impact with 12 fatalities (compare with Surowiecki and Taszarek, 2020) but it appears to be very difficult for realistic numerical prediction by contemporary operational convective-scale NWP model, as demonstrated below.



2.1 Synoptic overview

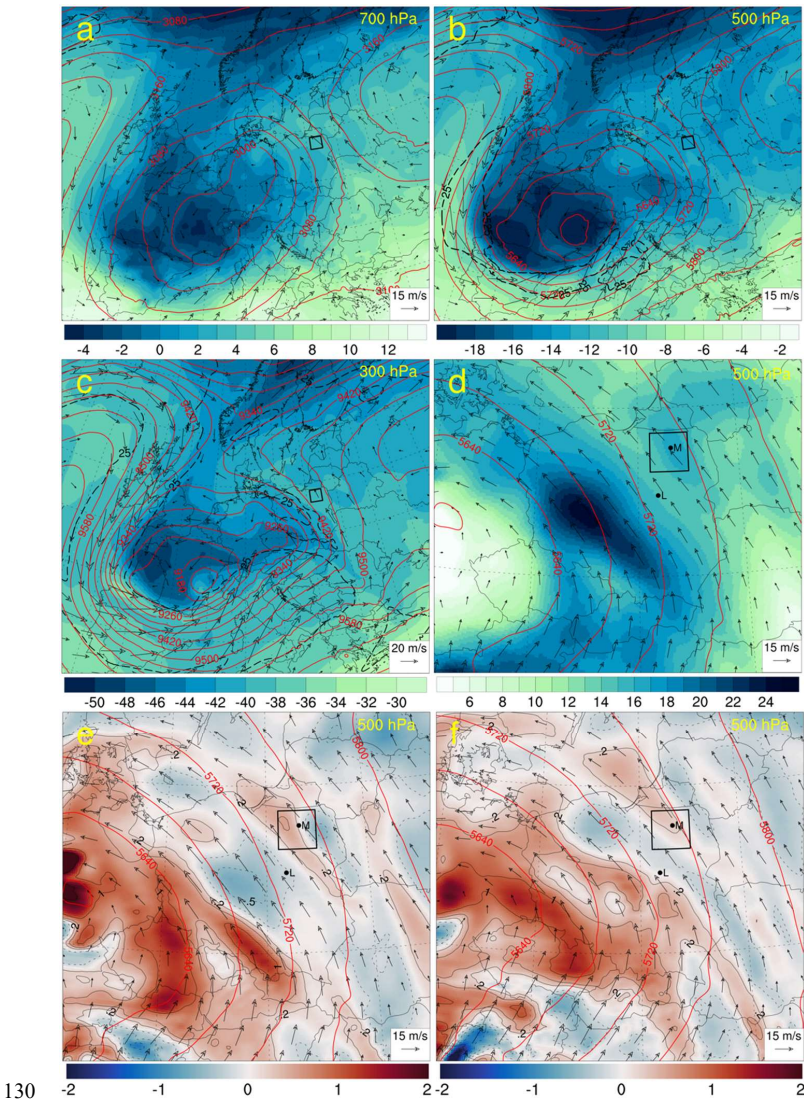


Figure 1: ERA-5 based analysis at 12:00 UTC, August 21, 2007: temperature ($^{\circ}\text{C}$ in colors), altitude (in m in red contours), wind vectors and 25 m s^{-1} isotach (black dashed contour) at 700 (a), 500 (b) and 300 hPa (c); (d) for wind speed (in m s^{-1} in colors), altitude and wind vectors at 500 hPa. Additionally, relative vorticity at 500 hPa is shown (in units 10^{-4} s^{-1} in color and contours at plus/minus 0.2, 0.5, 1.0, and 2.0 units, negative values are dashed) at 12:00 (e) and 15:00 UTC (f) of the day. The black rectangle indicates the area of convective development over northeastern Poland, and the black dots indicate the positions of weather stations at Legionowo (L) and Mikolajki (M).

On 21 August 2007, eastern Poland was covered by a warm subtropical Mediterranean air mass, away from the cold front situated near Poland's western border (not shown). The area was located between a deep cold upper-level low over western Europe and a warm ridge from over central European Russia (see Fig. 1 for ERA5-based analysis at 700, 500 and 300 hPa; the data are processed using int2lm preprocessor of the COSMO Consortium, Schättler and Blahak, 2021). A synoptic-scale tropospheric thermal gradient over Poland induced relatively strong upper-level southerly to southeasterly winds. At 12:00 (all hours are given in UTC and are presented in



the format HH:mm, where HH are hours and mm are minutes; 00:00 UTC corresponds with 02:00 Central European Summer Time), they reached 12–13 m s⁻¹ at 700 hPa and 16 m s⁻¹ at 500 hPa over northeastern Poland (see Fig. 1d for a localized band of higher wind in the area), but less than 14 m s⁻¹ at 300 hPa (the jet stream is located further southwest, Fig. 1c). Figures 1a and 1b indicate lack of notable warm advection at 700 and 500 hPa. Between 12:00 and 15:00, there is a prevailing weak negative relative vorticity advection at 500 hPa over the area (Fig. 1e and 1f), despite a distant presence of a short-wave trough approaching from the south. That suggests a weak dynamic suppression of deep convective activity over the area (following the omega equation interpretation, e.g., Holton, 2004).

2.2 Mesoscale conditions preceding severe convection development

Between 00:00 and 09:00 on 21 August 2007, northeastern Poland remained free from convective activity (not shown). The local synoptic weather stations (WSs) at Mikołajki and Kętrzyn (locations shown in Fig. 2b) reported night and early morning fog, and high morning 2-m dewpoint temperatures (T_d) in the range of 18 to 20°C. At about 06:00, the observed shallow cloud cover was between 2 and 6 octas, and quickly decreased later. Further presence of very moist air in the area was documented by a surface analysis at 12:00 (Fig. 2b), showing a relatively narrow moist plume covering Mikołajki (maximum T_d of 20.2°C) and elongated toward the north-northwest, towards Kętrzyn. With increasing daytime insolation and dissipating shallow clouds, the formation of a typical daytime well-mixed convective boundary layer (CBL) was expected over the area.

The vertical air-mass structure (Fig. 2a) was probed by the radiosonde ascent launched at 11:16 at Legionowo, 120 km southwest of the convection initiation area. The sounding showed an 800-m-deep well-mixed, but relatively dry (2-m T_d of 15.9°C) CBL capped by a layer with a reduced temperature lapse rate. Above, between 1250 m and 3300 m above mean sea level (AMSL), the sounding featured an almost-neutrally stratified elevated residual layer. Further above, up to about 5100 m AMSL, and around 7400 m AMSL, almost moist-neutral layers were also detected.

The wind speed increased with height from 1 m s⁻¹ at about 100 m AMSL to almost 10 m s⁻¹ at 650 m AMSL with east to south-southeast directions. Above, the wind speed increased from 9.5 m s⁻¹ at 700 hPa to 18 m s⁻¹ at 500 hPa and 23 m s⁻¹ at 300 hPa, and wind directions were from east-southeast to southeast. Moderate wind-speed shear of around 9 m s⁻¹ was observed between the surface and 700 hPa level, slightly above the 25 percentile for climatology of warm-season bow echo systems over Poland (Celiński-Mysław et al., 2018).

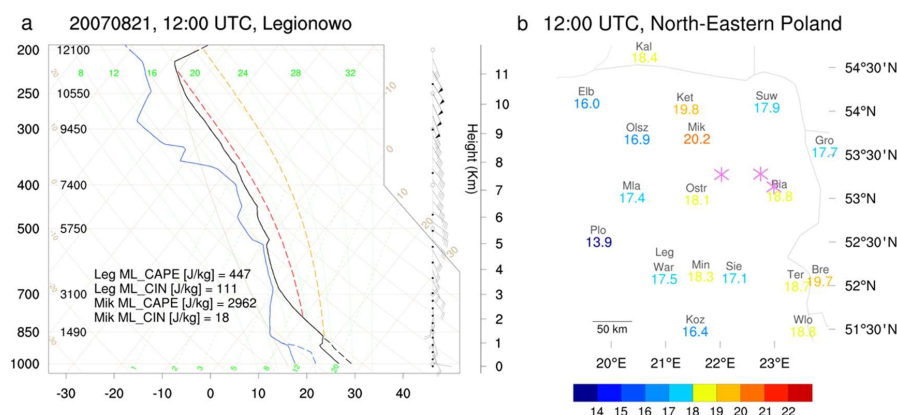


Figure 2: Skew-T diagram and wind (a, left) from Legionowo ascent on 21 August 2007 at 12:00 and (b, right) 2-m dewpoint temperatures (color scale and numerical values in °C) over northeastern Poland at that time. In (a), the black and blue continuous lines show T and Td (°C), respectively, and the black and blue dashed lines show T and Td reconstructed for CBL over Mikołajki (see text), respectively. The dashed red and yellow lines show results of pseudo-adiabatic ascent for Legionowo and Mikołajki, respectively. The resulting values of MCAPE and MCIN are shown in the lower-left corner of the figure. In (b), the abbreviations denote weather stations: Kaliningrad (Kal), Elbląg (Elb), Kętrzyn (Ket), Suwałki (Suw), Olsztyn (Olsz), Legionowo (Leg), Mikołajki (Mik), Grodno (Gro), Mława (Mla), Ostrołęka (Ost), Białystok (Bia), Płock (Plo), Warszawa (War), Mińsk Mazowiecki (Min), Siedlce (Sie), Terespol (Ter), Brest (Bre), Koźnice (Koz), and Włodawa (Wlo). Three purple asterisks mark the locations of the secondary convection initiation (compare Fig. 3).

The sounding-derived mixed layer parcel (with properties averaged over the lowest 500 m) convective inhibition (MCIN) was quite large at 111 J kg^{-1} , while the mixed layer parcel convective available potential energy (MCAPE) was relatively small at 447 J kg^{-1} , the latter significantly below the 25 percentile of MCAPE for warm-season bow echo systems over Poland of about 700 J kg^{-1} (Celiński-Mysław et al., 2018). Further northeast, however, the conditions were more supportive due to the observed significantly higher 2-m T and T_d (Fig. 2b). These conditions can be assessed by constructing a thermodynamic diagram linking well-mixed CBL characteristics estimated from local surface observations (following McGinley, 1986; and approximating CBL temperature and humidity profiles with dry adiabatic lapse rate and constant water vapor mixing ratio, respectively) and free tropospheric structure taken from the Legionowo sounding. Such a reconstructed sounding for Mikołajki (Fig. 2a, see also Wójcik, 2021) estimates MCIN and MCAPE at around 18 and 2900 J kg^{-1} , respectively, favoring strong convection.

2.3 Convection development

The deep convection initiation over northeastern Poland on 21 August took place outside the available radar range and is documented using Meteosat $10.8 \mu\text{m}$ imagery (Fig. 3). At 10:45, a strong primary convective cell was present south-southeast of Mikołajki with a cloud top of a few tens of kilometers wide having brightness temperatures below 220 K (Fig. 3a). The secondary convection initiated shortly before 11:00, with a new towering convective cloud (marked as 1 in Fig. 3b) seen immediately north of the primary cell. Subsequently, two convective cells developed nearby at 11:15, marked as 2 and 3 in Figure 3c. The anvils of the developing cells merged, producing at 12:00 an extensive ($\sim 100 \text{ km}$ across) cloud with a cloud-top temperature below 220 K.

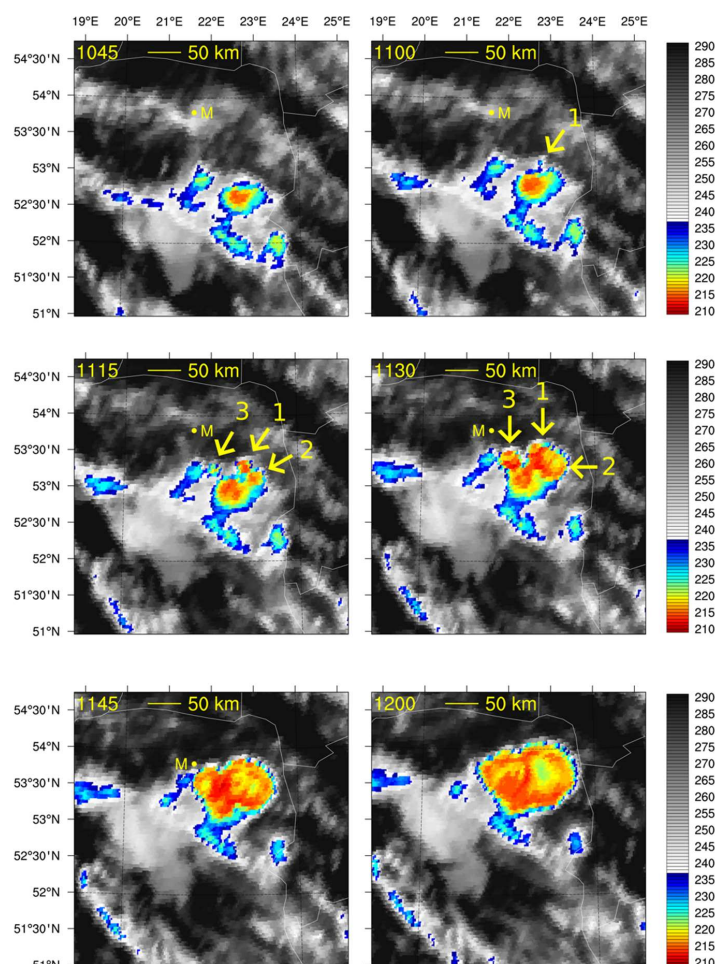


Figure 3: Convection initiation over northeastern Poland using brightness temperature derived from 10.8 μm channel observations of the Meteosat satellite (EUMETSAT). Numbers 1 to 3 denote individual towering cumulus clouds developing around 11:00 with arrows pointing toward the clouds. The yellow dot denotes the location of Mikolajki (M), the time in UTC is in the upper-left corner of every plate, yellow line shows a distance of 50 km.

The system moved towards northwest and, near 12:00, started to enter the range of the meteorological radar from Gdańsk (located west-northwest of the system). It indicated (Fig. 4) that the system's shape started to resemble the C-stage bow echo of Fujita (1978) around 13:00. That stage was also observed at 14:00 and 15:00. The radar-derived system propagation speed reached approximately 23 m s^{-1} between 13:00 and 14:20. The propagation direction (approx. 320°) agreed with wind direction in the Legionowo sounding at 700 and 500 hPa (Fig. 2) and was close to the orientation of the surface layer moisture plume, maintaining a moisture supply for the system development. The length of the bowing segment reached around 85 km at 13:30 and around 120 km at 15:00 (Fig. 4).

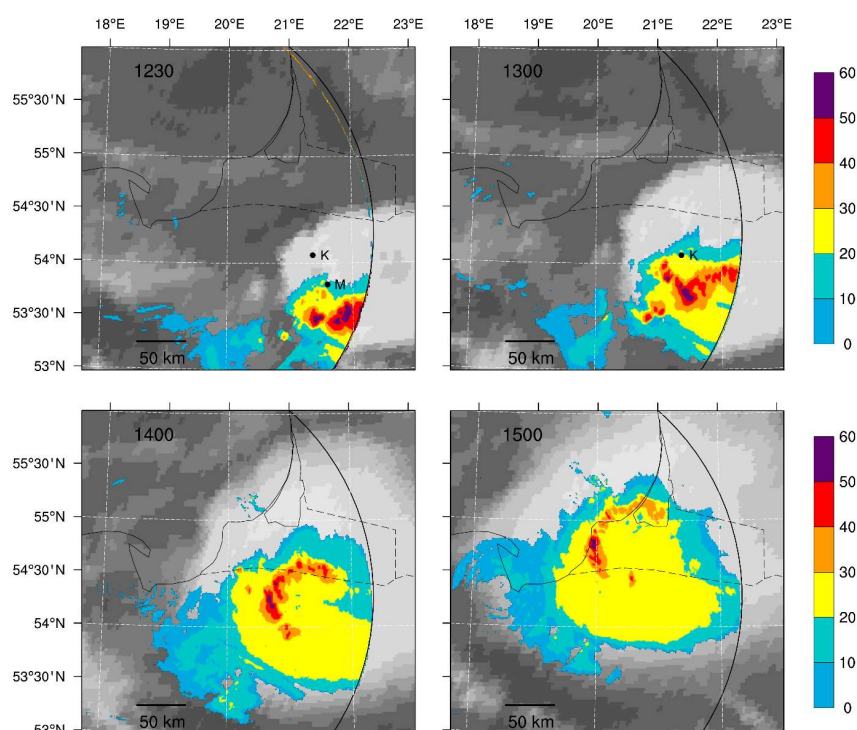


Figure 4: Radar reflectivity at 6.0 km altitude AMSL (color; dBZ) overlaid over the Meteosat 7.3 μm channel imaging (high/low upper-to-mid tropospheric water vapor concentrations marked with bright/dark colors; EUMETSAT). Black dots denote the locations of Kętrzyn (K) and Mikołajki (M).

2.4 Observations of the system passage

The Mikołajki WS recorded the convective system approach at 12:50, reporting very heavy rain shower and severe wind gusts (35 m s^{-1}). Hail was observed between 12:58 and 13:01. The total surface precipitation reached 24.6 mm. The 2-m temperature (T) dropped from 27.6 to 16.0°C, and 2-m T_d dropped from 20.2 to 15.5°C (these are shown as black symbols in Fig. 6a). Similar surface observations related to the system's passage were recorded at the Kętrzyn WS 20 minutes later, except for the lack of hail and with only 3.6 mm total precipitation. The strongest 10-m wind gusts reached 30 m s^{-1} (at 13:10), the 2-m temperature dropped from 26.6 to 17.7°C, and the dewpoint temperature dropped from 19.7 to 16.4°C.

WSs in Kaliningrad and Kaliningrad-Khrabrovo airport (Russian Federation) reported an approach of the system between 14:00 and 15:00 with much weaker maximum wind gusts of 16 m s^{-1} recorded at Kaliningrad WS. It reported total precipitation of 6 mm, 2-m T drop from 28.6 (at 12:00) to 19.7°C (at 15:00) and, analogously, 2-m T_d drop from 18.4 to 16.5°C.

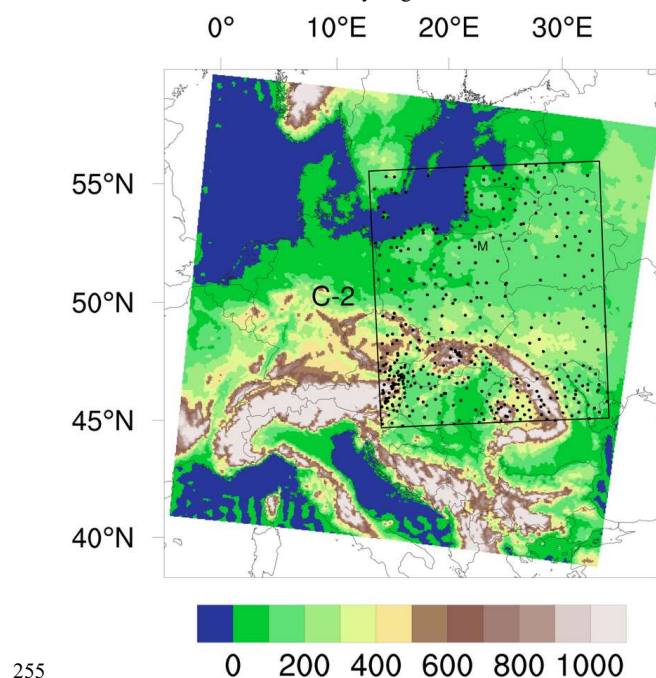
3 Data and tools for the numerical reconstruction of the convective system

Reconstruction of atmospheric environmental conditions is based on ECMWF ERA5 reanalysis. It applies 4DVAR-ensemble 12-hour-window global data assimilation (DA) of satellite, aeronautic, radiosonde, and selected surface observations, and an advanced land data assimilation system, coupled with IFS short-term global forecasts (Hersbach et al., 2020). We augment global ERA5 reanalysis with mesoscale DA following the



rationale discussed by Gustafsson et al. (2018). Our standard tool is the operational nudging (dynamic relaxation, see Anthes, 1974; Davies and Turner, 1977) of the COSMO Consortium (Schraff, 1997). The scheme works as a
240 non-linear 4-dimensional DA with a flexible time window. The scheme's design prevents the destruction of large-scale balances (e.g., by using sufficiently large time scales) and ensures balances within implemented observations (see extended discussion and technical details in Schraff and Hess, 2021). It has been successfully implemented for operational NWP by COSMO members (Baldauf et al., 2011) also for the assimilation of radar data with latent heat nudging (Stephan et al., 2008). It is also widely used for non-operational studies (e.g.,
245 Kienast-Sjögren et al., 2015; Bach et al., 2016; Wilhelm et al., 2023). Nudging methods are also used within ACCORD (Sass and Petersen, 2002) and WRF communities (e.g., Chen et al., 2018).

The main prognostic tool is an operational convective-scale NWP COSMO model (Baldauf et al., 2011) version 5.01 applying a 2.2 km horizontal grid spacing (C-2) implemented in the Institute of Meteorology and Water Management – National Research Institute in Poland. In the vertical, it uses 60 levels between the surface and
250 22.7 km AMSL, and a horizontal domain of 500 x 560 grid points (Fig. 5). Its IC/BC are dynamically downscaled from ERA5 data using the preprocessor int2lm and the convection-parameterizing COSMO 5.01 model with a horizontal grid spacing of 7.0 km (C-7). These IC/BC include three-dimensional wind velocity and thermodynamic variables with hydrometeors. BC are updated every 30 minutes. The model applies the same vertical structure but a horizontally larger horizontal domain of 310 x 310 grid points (Fig. 5).



255 **Figure 5: The COSMO computational domains: larger C-7 (with colored orography in m) and C-2 (black rectangle). Black dots show positions of assimilated weather stations including Mikolajki (M).**

C-2 and C-7 apply a single-moment cloud microphysical scheme with ice and snow (Reinhardt and Seifert, 2006) and with additional graupel for C-2, the multilevel TERRA soil model (Heise et al., 2003) and 2.5-
260 moment turbulence scheme with an advection of turbulent kinetic energy (Mellor and Yamada, 1982; Raschendorfer, 2001). The shallow and deep convection are parameterized (Tiedtke, 1989; Doms et al., 2021) in



C-7; there is no convection parameterization in C-2, except for two test experiments applying the shallow convection parameterization. The Ritter-Geleyn radiation scheme (Ritter and Geleyn, 1992) provides radiative tendencies updated every 15 minutes in C-7 and every 6 minutes in C-2.

- 265 The orography and surface parameters are derived independently for each resolution using the COSMO EXTPAR software (Asensio et al., 2020) and the leading databases for orography (ASTER; NASA/METI/AIST/Japan Spacesystems and U.S./Japan ASTER Science Team, 2019), land use (GlobCover; ESA GlobCover 2009 Project, 2010), soil type (HWSD; FAO/IIASA/ISRIC/ISS-CAS/JRC, 2012), and surface albedo (MODIS; Schaaf and Wang, 2015).
- 270 Configurations of the COSMO model and of the numerical experiments performed within the current study are summarized in Table 1.

Models	Description
C-7	$\Delta x=7$ km, 60 levels, IC and BC from ERA5 (except E7-C and E7-D), CP on
C-2	$\Delta x=2.2$ km, 60 levels, IC and BC from C-7, CP off (except EXSC)
Experiments	Description
E7-A	uses C-7, start 21. 07. 2007, 00:00, no further modifications
E7-B	uses C-7, start 20. 07. 2007, 00:00, nudging of soil observations
E7-C	uses C-7, start 21. 07. 2007, 00:00, soil IC from E7-B, atmospheric IC and BC from ERA5, nudging of soil observations
E7-D	Like E7-C, with additional atmospheric IC modification for low-to-mid tropospheric wind alteration
E2-A	uses C-2, start 21. 07. 2007, 00:00, IC and BC from E7-A, no further modifications
E2-B	uses C-2, start 21. 07. 2007, 00:00, IC and BC from E7-C, nudging soil and surface observations
EX	like E2-B, with additional surface heat fluxes correction
EXSC	like EX, with additional shallow convection parameterization
EX0S	like EX, with additional SCI of smaller horizontal size, single forecast
EX0 to EX8	like EX, but 9-member ensemble driven by additional SCI
EM	like EX, but atmospheric IC and BC from E7-D
EMSC	like EM, with additional shallow convection parameterization
EM0 to EM8	like EM, but 9-member ensemble driven by additional SCI

Table 1: Configurations of the COSMO model and of the numerical experiments performed within the current study; Δx stands for horizontal grid size, CP for convection parameterization and SCI for stochastic convection initiation.

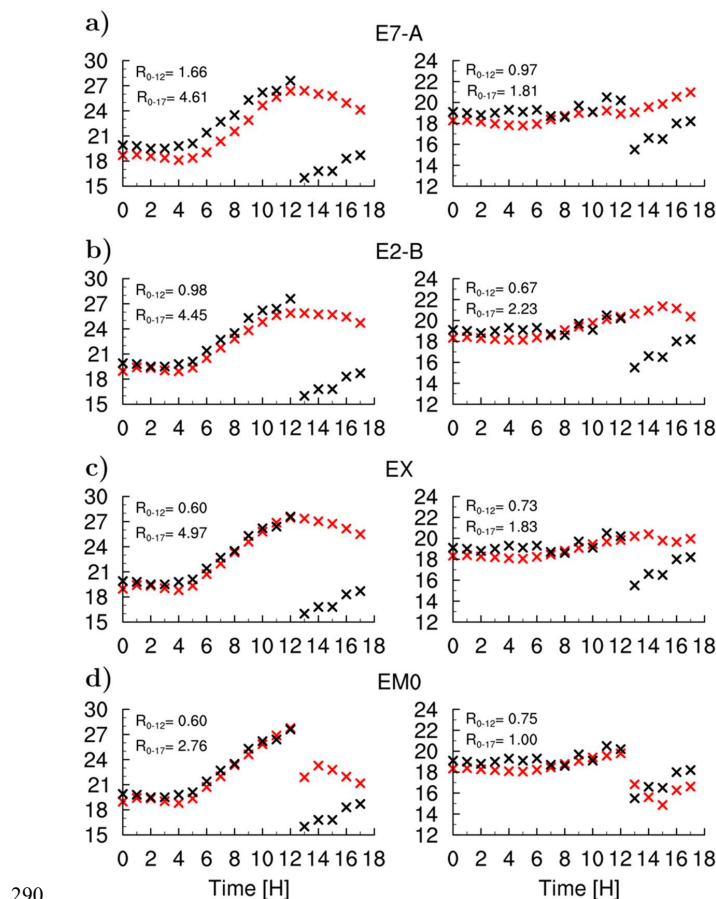
275 4 Initial conditions for convective-scale simulations and a correction of convective boundary layer characteristics

A successful numerical reconstruction of a severe convective system requires realistic environmental conditions supporting the system's development. That includes the temperature and humidity profiles within the atmospheric boundary layer (ABL) as they influence CAPE and CIN. Within the well-mixed CBL, these profiles



280 can be approximated as functions of 2-m T and T_d (McGinley, 1986) which makes the realistic evolutions of 2-m T and T_d good indicators of realistic temperature and humidity profiles across the CBL.

However, the C-7 simulation starting at 00:00 on 21 August 2007 with ERA5-based IC and BC (experiment E7-A, see Table 1) systematically underestimates the 2-m T and T_d over northeastern Poland during the whole pre-convective period between 00:00 and 12:00 (Fig. 6a for Mikołajki). The RMSE for the period are 1.66°C for T and 0.97°C for T_d for Mikołajki and 2.60°C and 1.01°C for Kętrzyn, respectively. Consequently, the simulated MCIN (around 40 J kg⁻¹) and MCAPE (around 2020 J kg⁻¹, not shown) over the area at 12:00 are notably overestimated and underestimated, respectively, compared to their observation-based estimates (Fig. 2a). The results of C-2 are similar (experiment E2-A), and the simulation does not develop deep convection in the area (not shown).



290 **Figure 6:** Comparison of the observed (black symbols) and simulated (red symbols) temperature (T; °C; left column) and dewpoint temperature (T_d ; °C; right column) evolutions for the Mikołajki WS on 21 August 2007: (a) E7-A simulation based on ERA5 data; (b) E2-B simulation with nudging of soil and surface observations; (c) EX-forecast with nudging and heat fluxes correction; and (d) EM0 simulation (section 7). Each panel shows the root mean square temperature errors (R) for periods 00:00-12:00 and 00:00-17:00 UTC.



4.1 Nudging of soil and surface observations

A possible reason for those model errors is a systematic underestimation of the soil temperature by 1 to 3°C (Wójcik, 2021). That bias is corrected in the simulation E7-B by nudging routine soil temperature measurements from 12 WSs in northeastern and eastern Poland (Mikołajki, Siedlce, Olsztyn, Białystok, Terespol, Mława, Elbląg, Suwałki, Warszawa-Okęcie, Koźnice, Włodawa, and Lublin). The measurements are converted to the model grid by Cressman's (1959) objective analysis with the radii of influence of 160 and 80 km for the first and second iterations, respectively. The nudging time scale is 60 minutes. The nudging starts the previous day (20 August) at 00:00 using C-7 with IC and BC from ERA5. Simulation E7-B provides the IC for soil temperature at 00:00 of 21 August for the corrected C-7 simulation starting at that time (E7-C).

The nudging continues within the main C-2 simulation (experiment E2-B) starting at 00:00 on 21 August and lasts until 13:00 with the soil IC taken from E7-B. The atmospheric IC and BC are downscaled from ERA5 using E7-C. The procedure is efficient, and reduces the soil temperature RMSE for the 5 WSs of the area (Mikołajki, Kętrzyn, Siedlce, Białystok, Olsztyn), from 2.75 to 0.6°C (calculated for these stations for 06:00 to 12:00 and soil depth of 10 to 20 cm). Lakes' effects are not parameterized within the model and are accounted for by defining the grid-scale surface temperature as an area average of the upper soil and constant lake temperatures applying the grid-scale fraction of the lakes' area. The lake temperature is 21.6°C, as measured at 05:00 on 21 August at the Mikołajskie Lake. The adjustment concerns the area located between 19 and 25°E, and 52 and 55°N.

The experiment E2-B involves also the COSMO nudging (see section 3) of SYNOP observations of 2-m T_d , 10-m wind, and surface pressure between 00:00 and 08:00. All available observations within the model domain (Fig. 5) are assimilated including hourly observations from Poland (77 stations) and 3-hourly observations from abroad (225 stations). However, E2-B still incompletely removes the pre-convective 2-m T and T_d errors: RMSE for Mikołajki (Fig. 6b) are 1.61°C and 1.07°C, and for Kętrzyn 1.88°C and 1.24°C, respectively.

4.2 Modification of surface heat fluxes

We hypothesize that, with simulated excessive morning cloud cover, the remaining biases are related to underestimated insolation and its impact on surface sensible and latent heat fluxes. Therefore, for the experiment EX, the insolation over northeastern Poland and western Belarus was increased to realistic values characteristic of the cloudless sky, following experiments performed within cloud-modeling and climate communities where cloud-radiation interactions are reduced or removed (e.g., Wu et al., 1998; Harrop et al., 2024 and references therein). The modification is active from 03:30 (approximate sunrise) until 12:00 but is locally turned off if convective precipitation is detected. The partitioning of the total surface heat flux into its sensible and latent components is corrected by altering the initial moisture content of the topmost 0.2 m deep soil layer following simulations investigating the influence of soil moisture on deep convection (e.g., Yamada, 2008; Gerken et al., 2015). Since the soil moisture measurements are not available, several plausible alternatives were tested to find soil moisture values that minimize the simulated 2-m T and T_d biases across 13 WSs in northeastern Poland (Białystok, Elbląg, Kętrzyn, Mikołajki, Mława, Olsztyn, Ostrołęka, Siedlce, Suwałki, Terespol) and western Belarus (Baranovichy, Grodno, Lida; see Wójcik, 2021, and especially table 5.2 therein for technical details). The applied corrections significantly improve the 2-m T and to a smaller degree T_d forecasts in the pre-convective period over northeastern Poland. RMSE for Mikołajki (Fig. 6c) is reduced to 0.61°C for 2-m T and is



0.73°C for T_d , and for Kętrzyn they become 1.32°C and 1.01°C, respectively. That brings the CAPE and CIN of EX close to values estimated from available observations, as discussed in the following section.

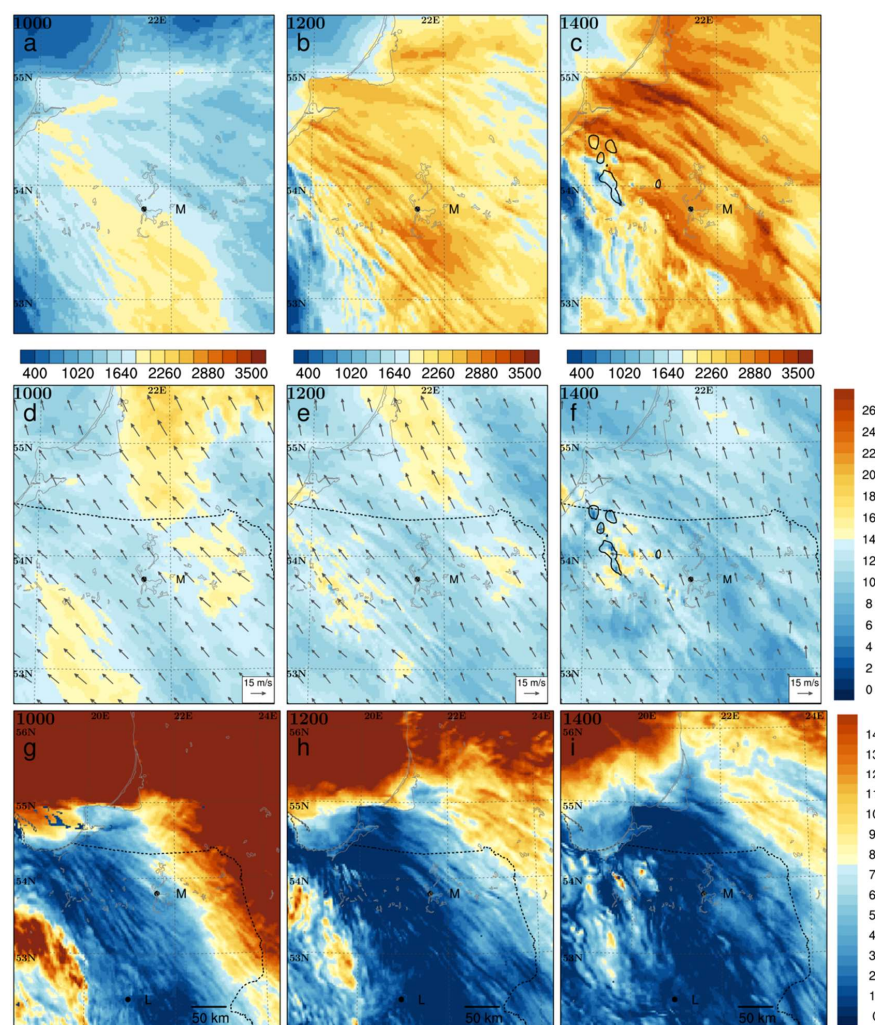


Figure 7: The environmental conditions in the vicinity of northeastern Poland on 21 August 2007 in EX-forecast: MCAPE (J kg^{-1} , top row), 100 to 3000 m vertical shear (m s^{-1} , second row), MCIN (J kg^{-1} , third row), all at 10:00 (left column), 12:00 (middle column) and 14:00 (right column); black contour shows pseudo-reflectivity of 30 dBZ at altitude of 3000 m, black dots show the positions of Mikolajki (M) and Legionowo (L).

5 Environmental conditions and deep convection in standard simulation with corrected boundary layer properties

The C-2 simulation with the corrected boundary layer characteristics, referred to as the EX-forecast, exposes the evolution of atmospheric environmental conditions over northeastern Poland (see Fig. 7 for MCAPE, shear, and MCIN; half-hourly analyses of MCAPE and shear in the supplement, Figs. S-1 and S-2). In the crucial period between 10:00 and 14:00 (Fig. 7 d to 7f), two nearly parallel bands of high low-tropospheric vertical shear (defined as the difference between the wind vectors at 3000 and 100 m AGL) locally reaching 17 m s^{-1} are



oriented along the shear direction and the wind at 3000 m, that is, from south-southeast toward north-northwest. Both bands shift slowly toward north-northeast and weaken. The area of prominent shear of at least 14 m s^{-1} within the band located southwest and west of Mikołajki slowly moves toward north-northwest and Mikołajki, gradually disintegrating.

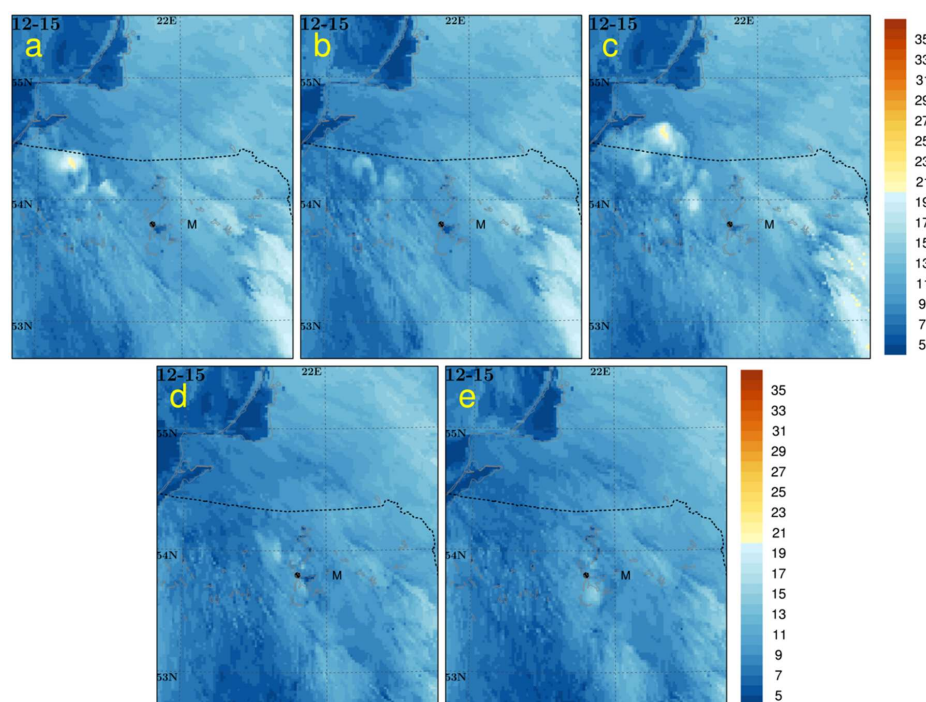


Figure 8: Maximum wind gusts between 12:00 and 15:00, 21 August 2007 (color scale in m s^{-1}) for: (a) EX-forecast (no CI); (b) EXSC-forecast (EX with shallow convection parametrization, no CI); (c) EX0S-forecast (CI like in EX0-forecast but for single-column CI perturbations, section 6); (d) EM-forecast (no CI, section 7); (e) EMSC-forecast (EM with shallow convection parametrization, no CI); black dot for a position of Mikołajki (M).

At 10:00 an irregular belt of high MCAPE reaching locally 2000 J kg^{-1} is elongated with the shear direction and located southwest and south of Mikołajki (Fig. 7a). With time (Fig. 7b and 7c), MCAPE increases and a vast area of MCAPE exceeding 2000 J kg^{-1} extends quickly toward northeast and north. Local maxima of MCAPE take the form of patches and filaments elongated along the shear and reach locally 2900 and 3300 J kg^{-1} south of Mikołajki at 11:30 and 13:30, respectively. A wide and stationary belt of low MCIN immediately west of Mikołajki is also elongated from south-southeast toward north-northwest (Fig. 7g to 7i). MCIN values within the belt diminish quickly with time and from 11:00 attain values below 10 J kg^{-1} in most of the belt's area.

Recent studies on deep convection initiation dynamics by Peters et al. (2022a; b) revealed that, despite earlier considerations, the high shear environment may promote the process. They showed that the high-shear-induced dynamic pressure perturbations adjacent to sufficiently developed thermals augment their further development instead of suppressing it. The deep convection (defined here as a presence of at least 30 dBZ pseudo-reflectivity at 3000 m AGL) develops in the EX-forecast in agreement with that scheme. The deep convection develops late, at 12:30 (Fig. S-1), and not in the highest CAPE and low CIN area, but where a belt of increased vertical shear exceeding 15 m s^{-1} coincides with a belt of locally increased MCAPE exceeding 2300 J kg^{-1} , about 80 km west of Mikołajki (Figs. S-1 and S-2). However, the convective gusts (calculated following Brasseur, 2001) do not



exceed 15 m s^{-1} until 14:30 and reach only 20 m s^{-1} by 15:00 (Fig. 8a). With additional lack of bow-shaped
375 convection organization (Fig. 7c), the simulation cannot be considered a successful representation of the actual
event.

Following a comment in Doms et al. (2021), the shallow convection parametrization was added to the model
configuration (experiment EXSC). That, however, did not improve the forecast: maximum convective gusts by
15:00 do not reach 20 m s^{-1} , being slightly weaker compared with the EX-forecast (Fig. 8b). There is also no
380 bow-shaped convection organization (not shown).

6 Convection initiation scheme and results of its application

The model's late deep convection initiation and failure in the development of the severe weather system despite
favorable environmental conditions suggest the lack of appropriate CI. Thus, an explicit CI scheme was designed
and applied. Its idea is to use near-grid-scale temperature perturbations, possibly resembling those physically
385 developing in CBL, and allow the model to explicitly represent further upscale growth of the perturbations. The
grid-scale perturbations are used in idealized cloud-scale studies (e.g., Tao and Soong, 1986; Grabowski et al.,
2006) or in cloud-resolving convection parametrizations (CRCP; Grabowski and Smolarkiewicz, 1999) used
within climate models (e.g., Ziemiański et al., 2005). The stochasticity of the method accounts for the limited
predictability of the flow at these scales (see Introduction).

6.1 Construction of the CI scheme

The first experiments using the temperature perturbations with a realistic amplitude of about $1.0\text{--}1.5^\circ\text{C}$ applied to
single grid columns did not improve the forecast (experiment EX0S, see Fig. 8c for maximum gusts). However,
if besides perturbing a single grid column, a 9% fraction of the temperature perturbation is applied to the four
neighbor grid columns (Fig. 9; analytical definition of the horizontal distribution of the temperature perturbation
395 within the perturbation range r_0 is $T_{\text{pert}}(r) = \Delta T \cos(r/r_0)$ for $r < r_0$, where ΔT is its amplitude at the central grid-
point, r is the distance between the central and a given neighbor grid-point, and $r_0 = 2.33 \text{ km}$), those
perturbations substantially impact the CI and are used within this study. The amplitude ΔT of the temperature
perturbation is drawn from the Gaussian distribution with a mean of 1.25°C and standard deviation of 0.5°C . The
perturbations stretch up between the surface and 760 m AGL. The horizontal perturbation size, arguably
400 resembling grid-scale thermals, is smaller than the model's effective resolution of about 7 horizontal grid
spacings (Fig. 5 in Ziemiański et al. 2021).

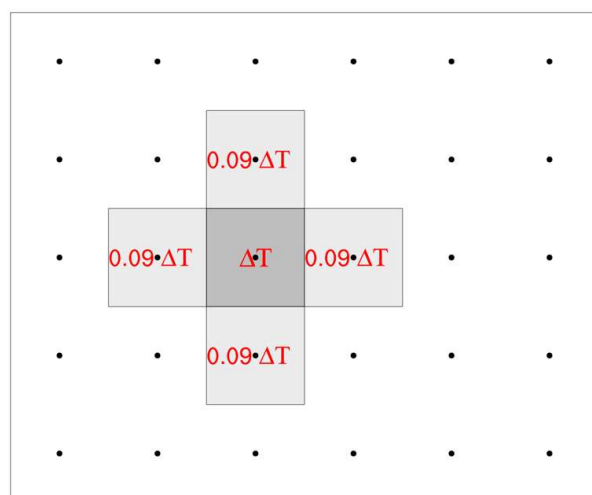


Figure 9: The horizontal structure of the temperature perturbation: black dots show the grid points' positions, shaded squares represent horizontal finite volumes of grid points with perturbed temperatures, and the value of temperature perturbation at a given grid point is in red.

The perturbations are activated over eastern and northeastern Poland between 09:30 and 11:30, during six 10-minute intervals. During every such interval, the perturbations are released at randomly chosen full minutes of the interval and their central columns are located at randomly chosen 4% of the grid columns of the area. Every active interval is followed by a 10-minute pause when the thermals are not released. If the 2-m temperature at the release point is lower than 23°C (a subjective threshold indicating a possible cold pool presence), the thermal is not released. Random configurations of the CI perturbations allow to form an ensemble of 9 forecasts (the size convenient for visualization and alike typically used 10-member ensembles, see Lawson and Gallus 2016 or Hirt et al. 2019), referred to as EX0 to EX8.



6.2 Impact of CI perturbations on environmental conditions

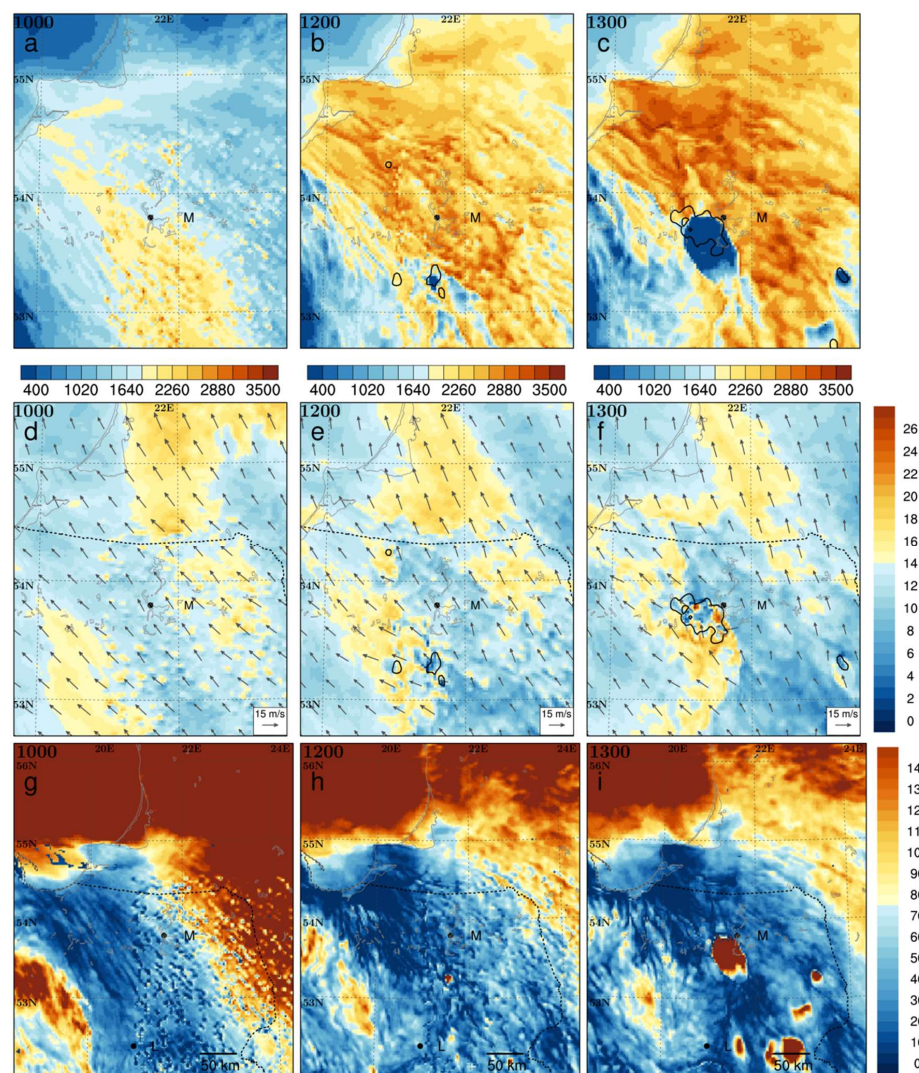


Figure 10: As Fig. 7 but for the EX0 ensemble member and the right column being for 13:00.

The implementation of CI notably influences the atmospheric environment (see Fig. 10 for the EX0 ensemble member; examples of half-hourly MCAPE evolutions for EX0 and EX3 members in Figs. S-3 and S-4). The increased temperature increases local buoyancy and CAPE and decreases CIN. However, rising thermals force compensating subsidence locally stabilizing the atmosphere. The MCAPE and MCIN spatial distributions in the CI area become grainy at 10:00 with local MCAPE maxima notably larger compared to the undisturbed environment (up to 2800 J kg^{-1} at 10:00 and 3300 J kg^{-1} at 11:30 in EX0). MCIN values locally diminish below 10 J kg^{-1} at 10:00. Larger-scale regions of high MCAPE (exceeding 2000 J kg^{-1}) in different ensemble members coincide generally with such regions of the undisturbed EX-forecast (not shown). With time, local MCAPE maxima form filaments and patches, different in location and strength for different ensemble members.



In the whole CI area, the vertical shear distribution (Figs. 10d to 10f; examples of half-hourly evolutions for EX0 and EX3 members in Figs. S-5 and S-6) becomes patchy at 10:00 with local maxima increased to $19\text{--}20\text{ m s}^{-1}$. Compared to the EX-forecast, the shear patches of at least 14 m s^{-1} within the high-shear band approaching Mikolajki from southwest reach further toward northeast (toward the high-CAPE area). The spatial extent of those patches becomes larger, and the shear maxima stronger, reaching 25 m s^{-1} by 12:30 for some members (EX6 and EX8, not shown). The mechanisms that alter the 3-dimensional wind distribution (and shear) are highly nonlinear and involve convective momentum transport and accelerations imposed by convective pressure perturbations (e.g., Wu and Yanai, 1994; Schlemmer et al., 2017; Dixit et al., 2021).

6.3 Development of deep convection and its cold-pool-driven dynamics

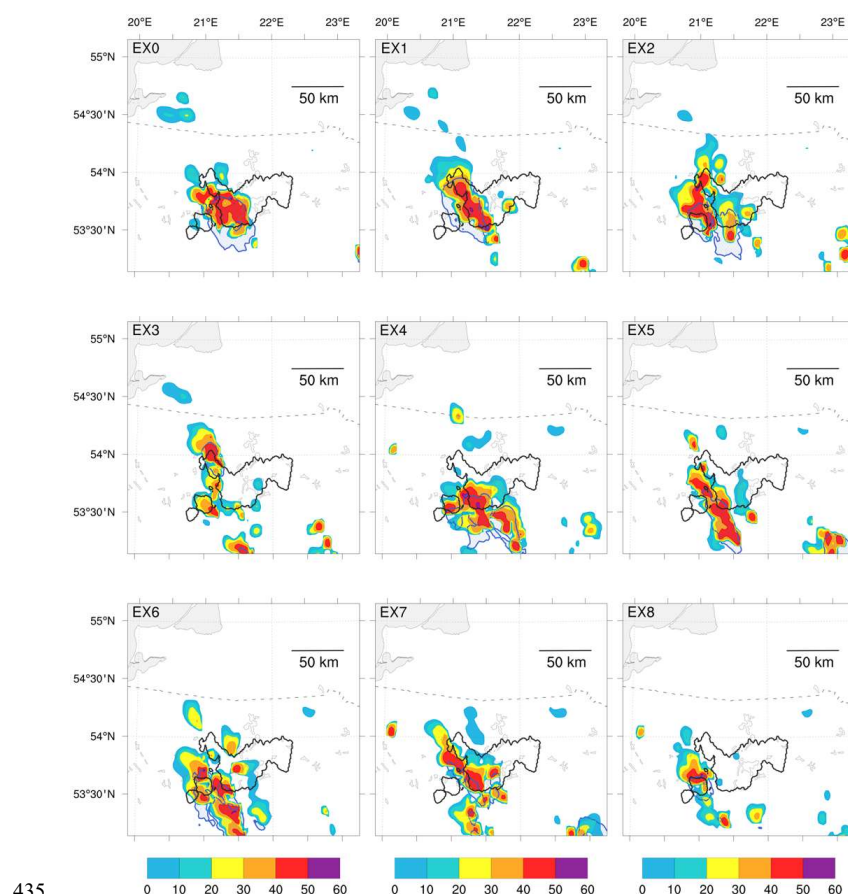


Figure 11: Simulated pseudo-reflectivity (dBZ, color scale) and cold pool extent (blue shading) for all EX-ensemble members at 13:00 (their numbers shown in upper-left corners) with area of the 30 dBZ reflectivity (black contour) of the observed system.

The first deep convective cells with pseudo-reflectivity reaching 30 dBZ at 3000 m AGL develop between 11:00 and 11:30 (depending on the ensemble member) in the area south, southwest and west of Mikolajki on locally increased CAPE features (Figs. S-3 and S-4 for EX0 and EX3). Some of those cells develop further, producing cold pools, sufficiently strong to significantly reduce MCAPE in the cells' area between 12:00 and 13:00 (e.g., Fig. 10c), and severe gusts, later. In those cases, the process begins where the high-shear patches (at least 14 m s^{-1}



¹), located within the eastern edge of the high-shear band heading toward Mikolajki from southwest, approach
445 the high CAPE features (Figs. S-3 to S-6 for EX0 and EX3). That strongly suggests the decisive role of high
shear via a mechanism discussed by Peters et al. (2022a; b) in the early development of such deep convection
systems.

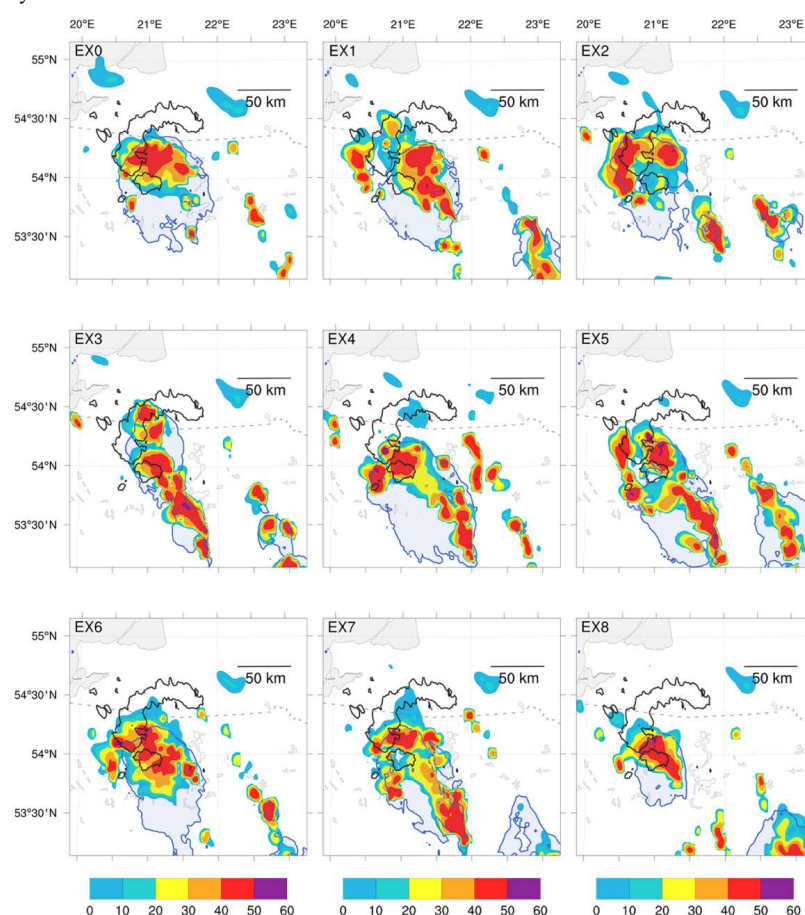


Figure 12: As Fig. 11 but at 14:00.

450 At 13:00, all ensemble members produce clusters of deep convective cells in the vicinity of the observed system
(Fig. 11). They are not yet organized into bow-shaped systems but have developed deep cold pools (see Table 2;
the cold pools' temperature depression is calculated for the 2-m T relative to the EX-forecast). By 14:00, the
cold pools intensify (Table 2), and all ensemble members feature the convective clusters with cells located in the
vicinity of the cold pools' leading edge, for most of them (EX0, EX2, EX4, EX6, EX7, EX8) along a bow-
455 shaped line (Fig. 12). The latter suggests the presence of cold-pool-driven dynamics in the development of the
clusters, even though the cells tend to be separated from each other.

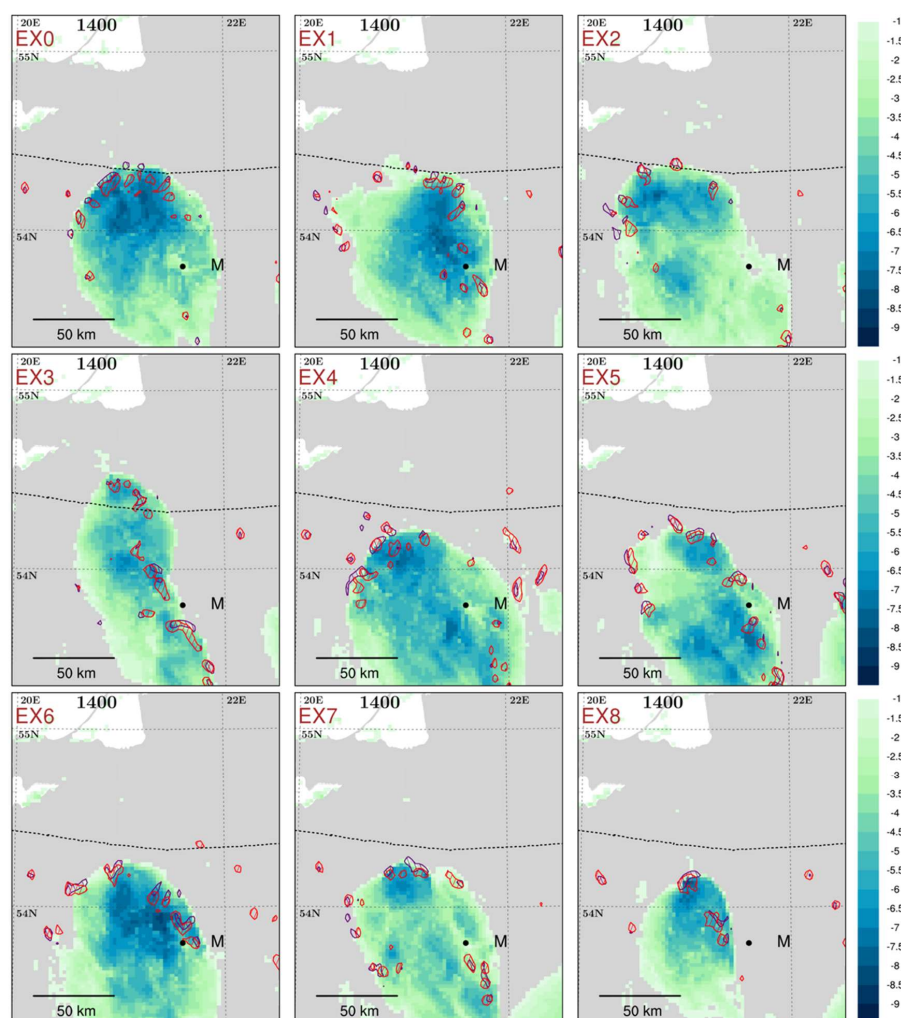


Figure 13: 2-m temperature depression (color, °C; see text for definition) and the isolines of 5 m s^{-1} vertical wind at an altitude of 3 km AMSL (violet hatching) and 6 km AMSL (red hatching) for all EX-ensemble members (numbers in upper-left corners) at 14:00; black dot for the position of Mikolajki (M).

That is verified by Fig. 13 showing the cold pool temperature depression and positions of convective updrafts stronger than 5 m s^{-1} for all ensemble members. The figure indicates that all ensemble forecasts feature strong convective updrafts located along the cold pool's leading edge, thus confirming that the convective clusters of all ensemble members are subjected to the cold-pool-driven dynamics despite the individual updrafts being isolated and not forming a compact linear structure. Further confirmation comes from the subsequent evolution of all the systems (Fig. S-7 for 14:30) that keep developing strong updrafts (which tend to increase in number and spatial extent) on the cold pools' leading edges. At 14:00, the cold pools' leading edges and the related convective clusters are located relatively close to the actual system's position but –except EX3– stay clearly behind it (Fig. 12).



Ensemble members	EX0	EX1	EX2	EX3	EX4	EX5	EX6	EX7	EX8	Av.
Max gusts by 13:00 UTC	25	18	20	18	24	16	18	19	18	20
Max gusts by 14:00 UTC	30	30	25	25	29	26	30	23	33	28
Max 2-m T depr. at 13:00 UTC	7.5	6.6	6.8	5.5	7.7	6.5	6.5	5.2	5.2	6.4
Max 2-m T depr. at 14:00 UTC	8.4	8.2	8.0	7.2	8.0	7.9	8.8	7.3	8.6	8.0

Table 2. Maximum gusts (m s^{-1}) at half-hourly periods between 12:30 and 13:00, and between 13:30 and 14:00 UTC, and cold pool amplitudes ($^{\circ}\text{C}$) at 13:00 and 14:00 UTC for all members of EX ensemble with ensemble averages.

By 14:00, four ensemble members produce maximum gusts between 23 and 26 m s^{-1} and five members between
475 29 and 33 m s^{-1} (Table 2). Figure 14 shows the spatial distribution of maximum gusts between 12:00 and 14:30
for all ensemble members and relates them to the distribution of available damaging wind reports. While none of
the forecasted areas of gusts of at least 20 m s^{-1} covers the whole area of damaging wind reports, most of these
simulated areas are relatively close or cover at least part of the damaging wind area (EX0, EX1, EX3, EX4, EX5,
and EX6). There is an overall tendency to develop strong gusts further west and north compared to their actual
480 position. That is at least partly related to a model's delay in the gusts' development. Overall, however, the
implementation of the CI scheme radically improves the forecast making it comparable to the observed system.

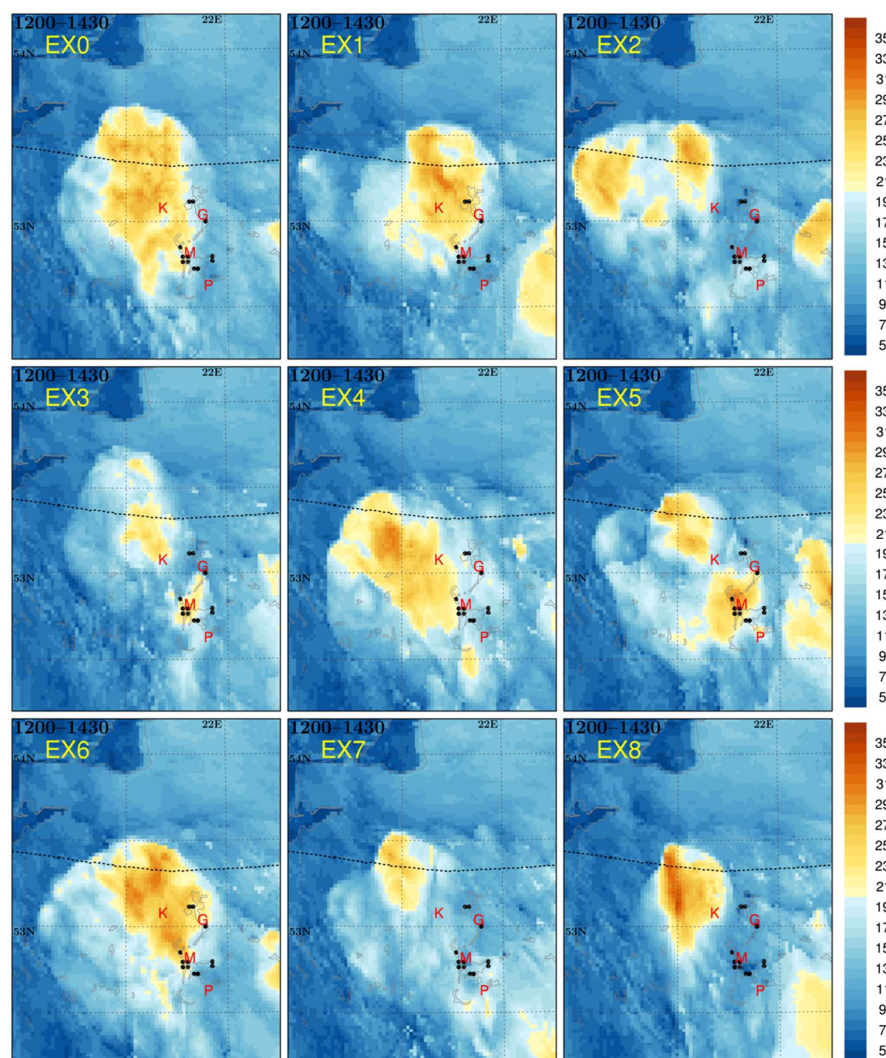


Figure 14: Spatial distribution of maximum 10-m wind gusts (m s^{-1}) in the period between 12:00 and 14:30 for all members of EX-ensemble with positions of towns with damaging winds reports (based on press releases) marked by red capital letters and positions of death reports marked by black dots.

7 Increased-shear experiment

There are no observations directly verifying the lower-to-mid-tropospheric wind velocities simulated within the high-wind band over the Mikołajki area during the convective development. However, the simulated slower propagation of the convective cluster between 13:00 and 14:00 (see previous section) allows us to hypothesize that the velocities are underestimated in the model simulations (e.g., Weisman and Klemp, 1986). One may expect that thermal wind relation played a role in the development of those winds (Fig. S-8 for 850-500 hPa thickness evolution). Such a conjecture suggests an experiment to increase wind velocity within the band (and



thus increasing the vertical shear) and tests the impact on the simulated convective system's strength, morphology, and timing. The wind is strengthened by increasing its balanced component via local strengthening of the low-to-mid-tropospheric horizontal temperature gradient.

7.1 Shear modification technique

The experiment is set up via appropriate modifications of lower-to-mid-tropospheric temperatures in the source area of air that departs at 00:00 and reaches the colder/warmer (western/eastern) side of the band over Mikołajki around 12:00. The modifications are implemented within the E7-D experiment that provided the IC and BC for the convective-scale experiment EM. To keep the experiment within realistic bounds, the applied temperature modifications, albeit arbitrary, are bounded by available upper-air observations.

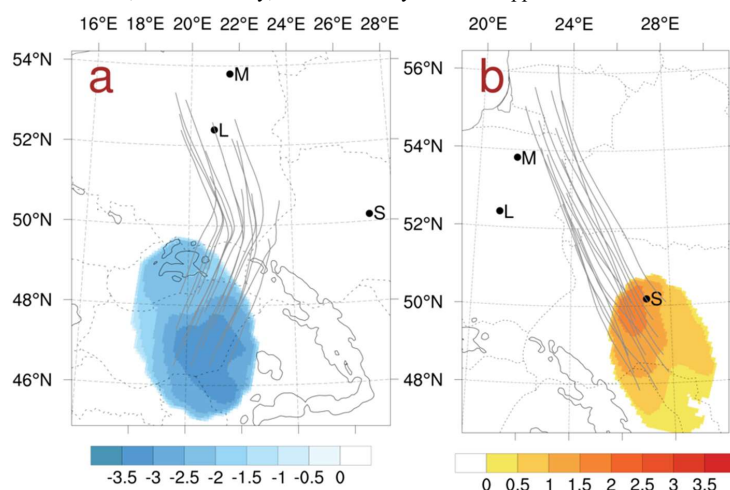


Figure 15: The areas of temperature modification and its value (°C, color) together with forward parcel trajectories between 00:00 and 12:00 of 21 August 2007 for (a) negative temperature modification at 650 hPa and (b) positive temperature modification at 700 hPa. M, L and S mark locations of Mikołajki, Legionowo and Shepetivka.

The temperature modifications for the eastern side of the increased temperature gradient are performed in the source area of trajectories arriving east of Mikołajki at 12:00, located near and south of the Shepetivka upper-air station (Fig. 15b, see also Fig. S-9; the trajectories are calculated with Lagranto software following Sprenger and Wernli, 2015). The modification area is contained between 900 and 520 hPa and has the form of an ellipse having foci located at 27.05°E, 50.18°N, and 28.10°E, 47.25°N; the semi-major axis equals 201 km. The temperature is increased to measurements from Shepetivka sounding at 00:00 and is horizontally uniform over the area. Additionally, the humidity in the area is reduced to values close to those observed at Shepetivka (Fig. 16d) to avoid triggering spurious morning convection.

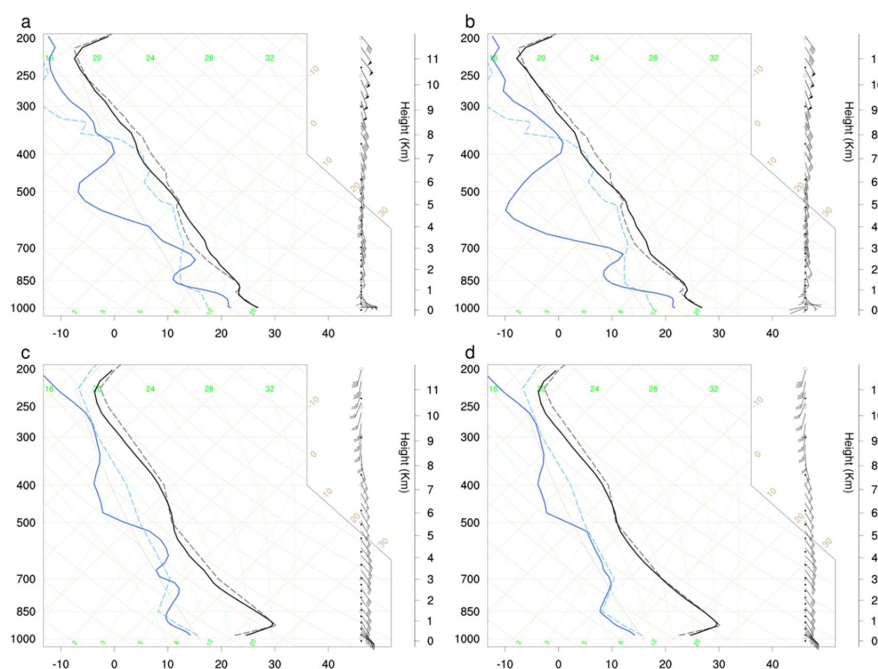


Figure 16: Model-derived aerological sounding for Legionowo at 12:00 on 21 August 2007 without lower-to-mid tropospheric temperature modification (a) and with the modification (b), and for Shepetivka at 00:00 on 21 August 2007 without lower-to-mid tropospheric temperature and humidity modifications (c) and with the modifications (d); T in black and T_d in blue lines. The observations at respective stations are shown using dashed lines.

The modifications for the western side of the increased gradient zone are performed in the source area of trajectories arriving near the Legionowo upper-air station at 12:00 (Fig. 15a, see also Fig. S-9). The modification area is contained between 830 and 540 hPa and has a form of ellipse with foci located at 19.60°E, 48.95°N, and 20.90°E, 45.85°N; and its semi-major axis equals 225 km. The modified temperature is horizontally uniform. There is no representative upper-air station in the area, so the temperature is lowered to make the simulated temperature profile at Legionowo at 12:00 closer to the observed one. With modification amplitudes slightly stronger compared to those around Shepetivka (up to -3 °C compared to 2.5 °C, Fig. S-9), the Legionowo temperature in the lower-to-mid troposphere was reduced on average by 0.7 °C and is closer to observations (Fig. 16b). The model quickly recovers the balance and increases the horizontal temperature gradient over the severe convection area around noon (Fig. S-8).

7.2 Impact of shear modification on environmental conditions and deep convection without CI

As expected, the modifications influence mainly the vertical shear amplitude in the EM-forecast while preserving its overall mesoscale pattern over northeastern Poland between 10:00 and 14:00 (Fig. S-10 to compare with Fig. 10, and Figs. S-11 and S-12 to compare with Figs. S-1 and S-2). In the EM-forecast, as in the basic EX-forecast, the shear slowly weakens with time but remains stronger by 2-3 m s⁻¹ in most of the area, locally even by about 5 m s⁻¹, compared to the EX-forecast. The thermodynamic conditions are also alike, including MCIN and MCAPE overall patterns. The distribution of MCIN values, smaller than about 10 J kg⁻¹, is similar, and while MCAPE values tend to be slightly lower over most of the area (by approximately by 100 J kg⁻¹), local maxima near Mikołajki tend to be larger by 100-200 J kg⁻¹.



In the EM-forecast without stochastic CI, deep convection develops at 13:00 about 40 km south of Mikołajki (Fig. S-11), that is, in a different area and half an hour later than in the EX-forecast. Convection develops in the area where a narrow belt of shear reaching 17 m s^{-1} catches up with a narrow belt of MCAPE exceeding 3000 J kg^{-1} (Figs. S-11 and S-12), in agreement with the dynamics discussed by Peters et al. (2022a; b). Compared to the EX-forecast, the maximum convective gusts are weaker (down to about 15 m s^{-1} by 15:00, Fig. 8d) despite convection developing within the area with stronger CAPE and shear (compared to the EX-forecast). Also, augmenting the forecast with additional shallow convection parameterization (experiment EMSC) does not improve the forecast (see Fig. 8e for maximum gusts). Overall, the increase in shear alone did not improve the severe weather forecast.

7.3 Impact of shear modification on environmental conditions and deep convection with the CI

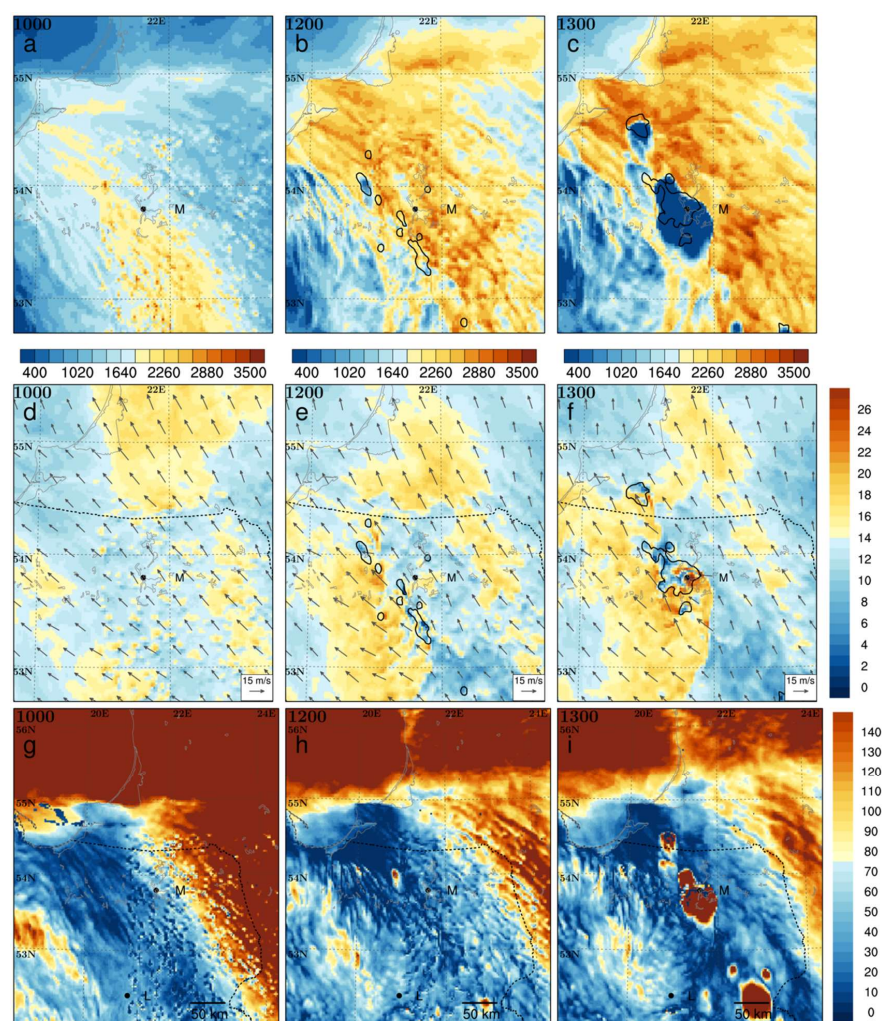


Figure 17: As Fig. 10 but for EM0 ensemble member.



Next, the saved configurations of the stochastic CI used to generate ensemble members EX0 to EX8 are used within the increased-shear environment to generate a new EM-ensemble with members EM0 to EM8. As in the EX-ensemble, the implementation of CI alters the distribution of environmental parameters, making their small-scale structure grainy or patchy (see Fig. 17 for the EM0 member, and Figs. S-13 to S-17 for example members EM0 and EM3). Compared to the analogous EX-ensemble members, the local shear maxima are stronger by 1-3 m s⁻¹ already at 10:00. They quickly increase and reach 24-25 m s⁻¹ by 11:00 in most of the ensemble members. Values of local MCIN minima (below 10 J kg⁻¹) and local MCAPE maxima are similar in both ensembles. Small-scale structures of MCIN and shear are at first similar for the analogous members of both ensembles but diverge from about 11:00 for shear and 12:00 for MCIN.

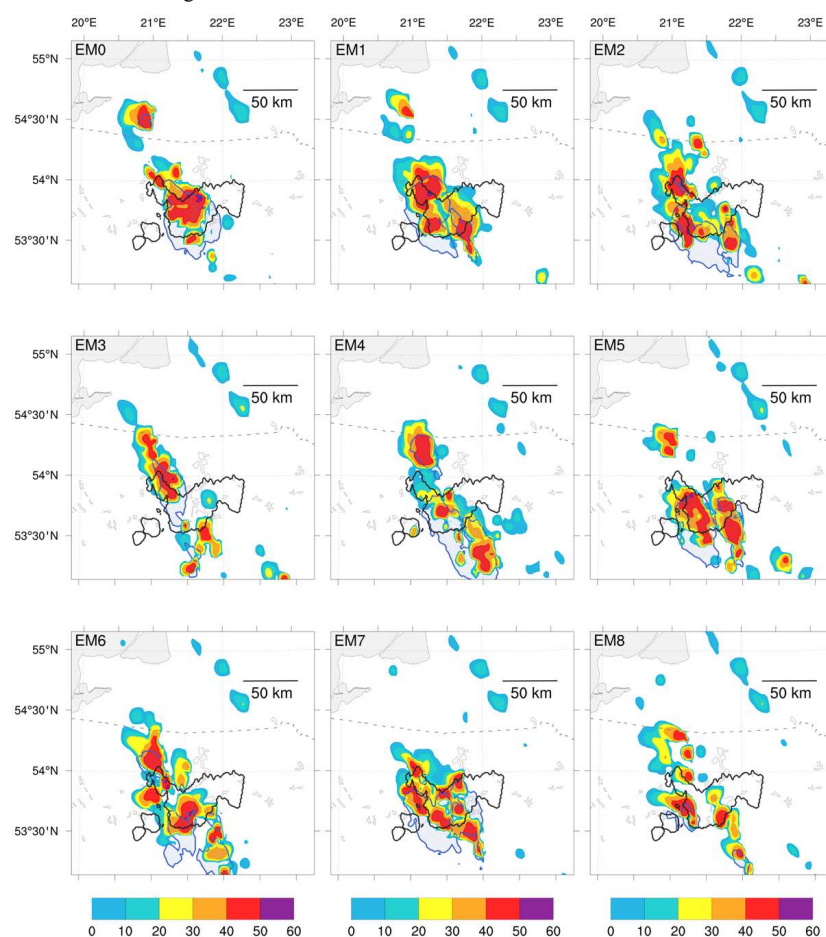
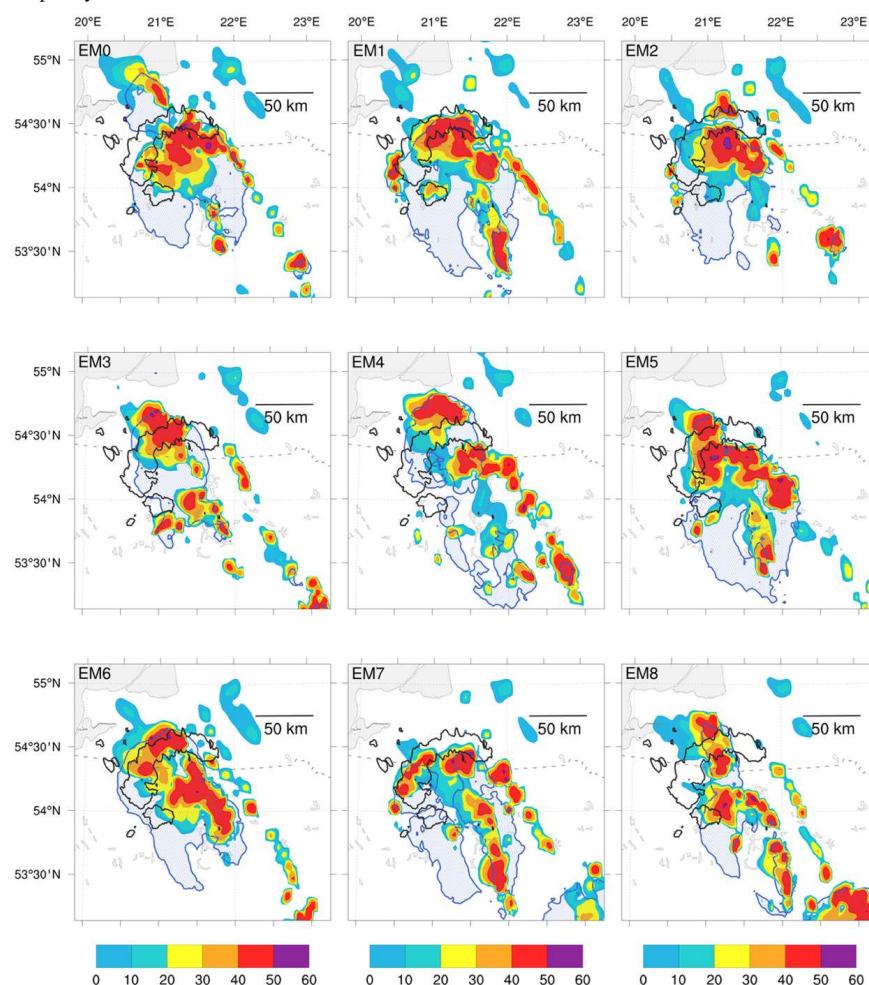


Figure 18: As Fig. 11 but for the EM ensemble.

Deep convective cells (pseudo-reflectivity reaching 30 dBZ at 3000 m AGL) develop earlier (between 10:30 and 11:00) in the EM-ensemble (example Figs. S-13 and S-14). Intensive developments take place where the locally increased shear patches (at least 14 m s⁻¹) approach the increased CAPE features (Figs. S-13 to S-16), as in the EX-ensemble. Already at 13:00, all EM-ensemble members produce clusters of deep convective cells with deep cold pools (Table 3; the cold pools' temperature depression is calculated for the 2-m T relative to the EM-



forecast) in the close vicinity of the actual system's position (Fig. 18), but the cells are not organized into bow-shaped systems.



570 **Figure 19: As Fig. 12 but for the EM ensemble.**

By 14:00, all ensemble members feature convective clusters with cells located in the vicinity of the cold pool leading edges, and all but EM3 along a bow-shaped line (Figs. 19). Compared to the EX-ensemble, there are more such ensemble members, and the cold pools tend to be more widespread. Moreover, the convective clusters are located closer to the position of the observed system, indicating improvement in the system's propagation speed.

575

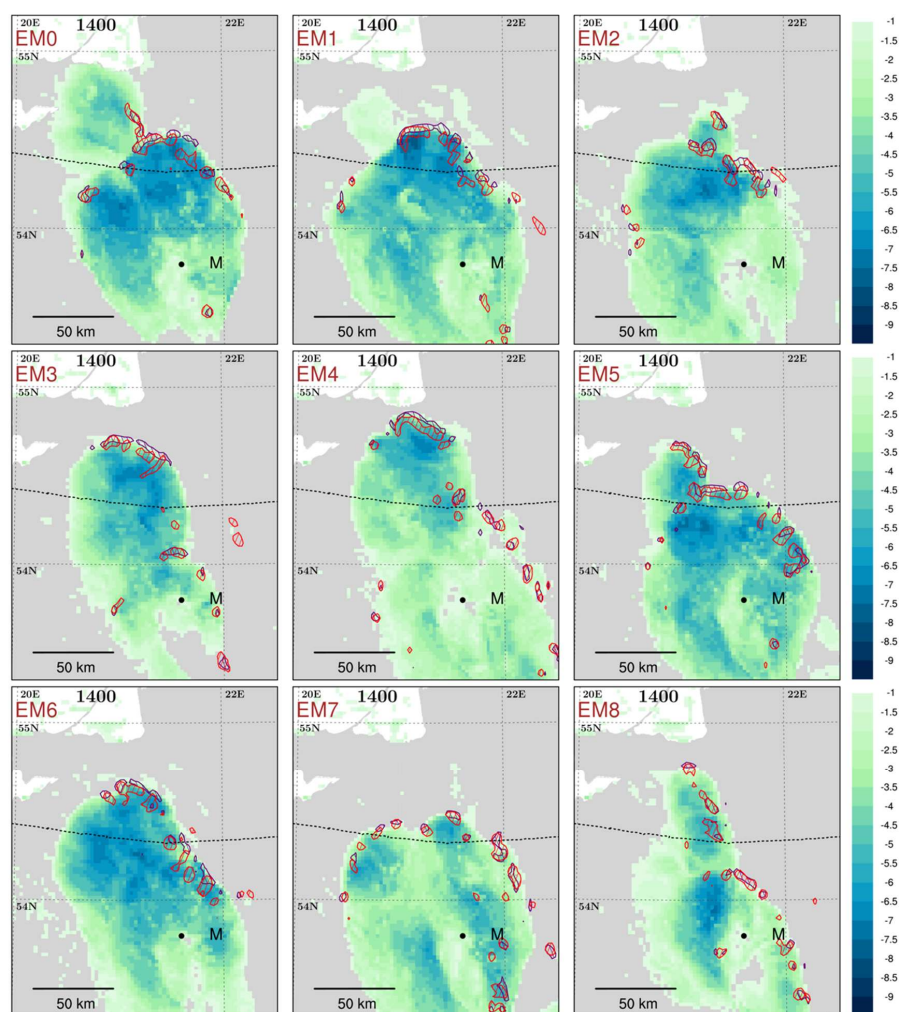


Figure 20: As Fig. 13 but for the EM ensemble.

Figure 20, analogously to Fig. 13, indicates that all EM-ensemble members feature strong convective updrafts organized along the cold pool's leading edges, confirming the cold-pool-driven dynamics of these convective systems. The updrafts tend to be more widespread compared to the EX-ensemble members, some forming lines of 10-km-length scale. For some of the ensemble members, the cold pools attain a more complicated dual structure, with the updrafts forming at the leading edges of both parts (EM2, EM3, EM4, EM5, EM7, EM8). Later, for all ensemble members, the convective systems keep developing strong updrafts on the cold pools' leading edges, confirming a persistence of the cold-pool-driven dynamics (Fig. S-17 for 14:30).

585

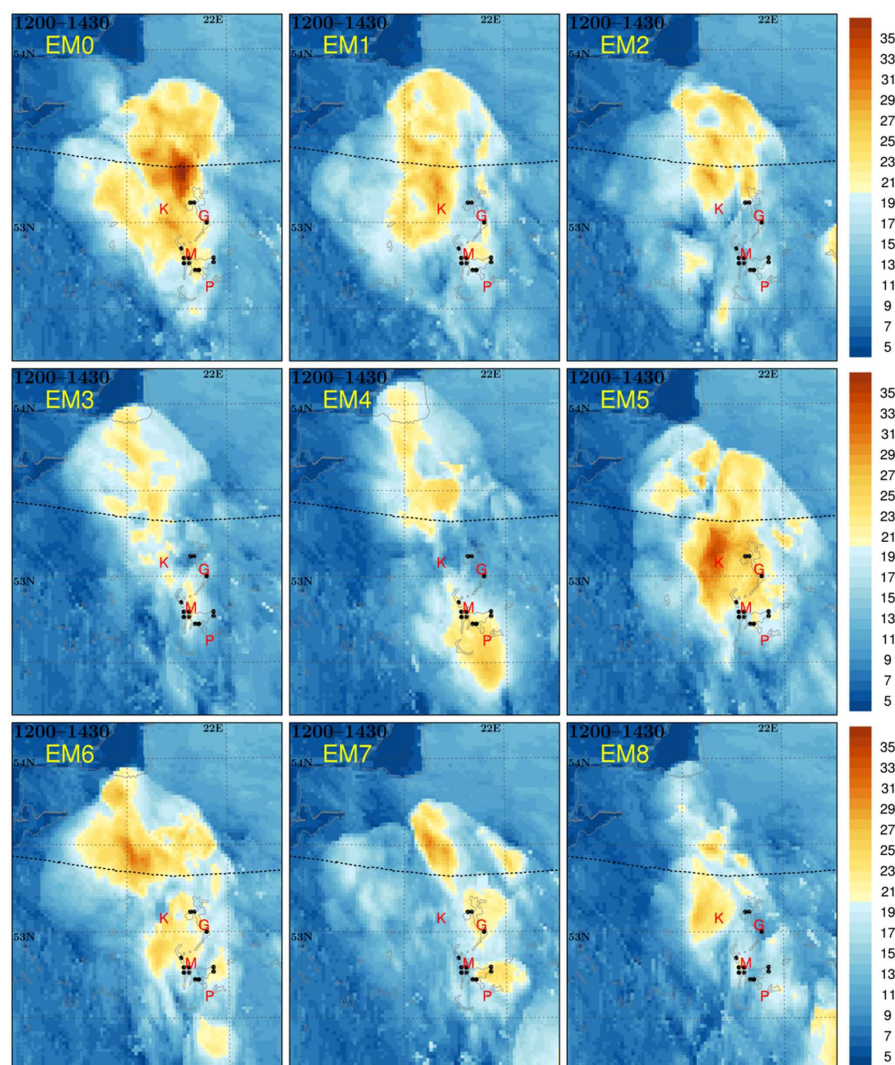


Ensemble member	EM0	EM1	EM2	EM3	EM4	EM5	EM6	EM7	EM8	Av.
Max gusts by 13:00 UTC	24	26	23	18	27	26	23	17	15	22
Max gusts by 14:00 UTC	38	29	30	25	24	34	31	28	27	30
Max 2-m T depr. at 13:00 UTC	7.7	7.1	6.9	6.1	7.3	8.1	6.8	7.1	5.8	7.0
Max 2-m T depr. at 14:00 UTC	7.9	8.5	7.9	7.3	7.3	7.9	7.7	6.5	7.6	7.6

590 **Table 3. Maximum gusts (m s^{-1}) at half-hourly periods between 12:30 and 13:00, and between 13:30 and 14:00 UTC, and cold pool amplitudes ($^{\circ}\text{C}$) at 13:00 and 14:00 UTC for all members of EM ensemble with ensemble averages.**

The maximum gusts in the EM ensemble are stronger compared to the EX-ensemble (Table 3), with four ensemble members producing maximum gusts between 25 and 28 m s^{-1} and five members between 29 and 38 m s^{-1} . Also, the spatial distributions of maximum gusts between 12:00 and 14:30 tend to be closer to reality (Fig. 21). EM0 and, to a large degree, EM5 have gusts of at least 20 m s^{-1} covering the area of damaging wind reports, and such gusts of all members but EM2 cover at least some of that area. There is still a tendency to forecast strong gusts further west and north (at least partly related to a slower spin-up of simulated convective processes) compared to their actual position.

595



600 **Figure 21: As Fig. 14 but for increased shear ensemble EM.**

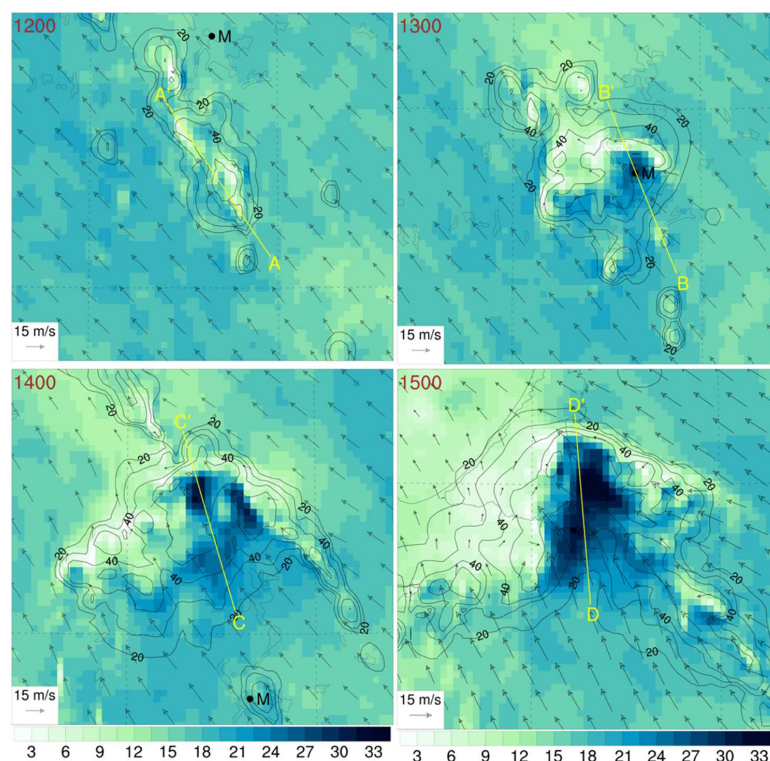
The forecast ensemble using the CI responds well to the increase of low-to-mid tropospheric wind and shear via increasing the maximum gusts of the ensemble and convective system propagation speed while making the spatial structure of convective cells and updrafts more bow-echo-like.

8 Rear inflow jet in the EM0 forecast

605 In the EM0 forecast, the timing and position of the convective system most closely resemble the observations, and wind gusts in the period between 13:00 and 14:00 are the strongest (38 m s^{-1}). Therefore, a brief analysis of the influence of convective processes on the low-to-mid tropospheric flow is performed for that forecast, assuming that it may give the best approximation to the real development. Figure 22 shows the 700-hPa wind in the vicinity of the developing convective cluster. The figure indicates that there is no significant wind increase



610 close to the convective cells at 12:00. At 13:00, the wind speed increases in the rear part of the strong echo area, reaching 29 m s^{-1} in a small area above Mikołajki. At 14:00, the local area of the strongest wind reaching 33 m s^{-1} increases forming two patches. Only at 15:00, a relatively large and compact area of strong wind reaching 36 m s^{-1} is seen suggesting a presence of a well-developed RIJ.



615 **Figure 22:** Wind speed (color scale in m s^{-1}) and wind vectors at 700 hPa in the vicinity of the convective cluster with column-maximum pseudo-reflectivity (CMAX, dBZ in black contours), hour in UTC in left upper corners. The black dot shows the location of Mikołajki (M), and the yellow lines show the positions of cross-sections; their length is 65 km.

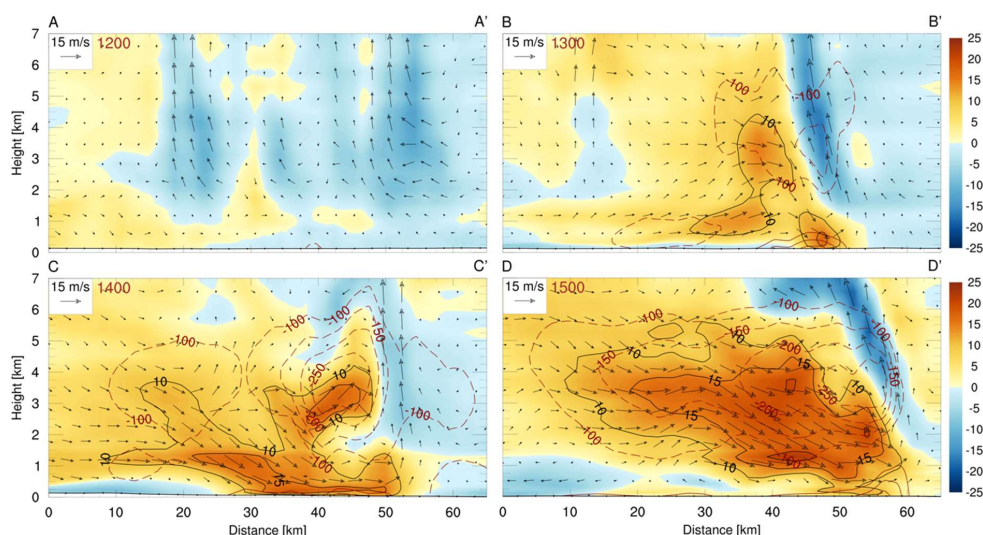


Figure 23: Vertical cross-sections through horizontal wind perturbation relative to reference EM-forecast; its component along the direction of the reference wind averaged over the cross-section in 700-500 hPa layer is shown (color scale and black isotachs at 10, 15 and 20 m s⁻¹), black vectors show the horizontal and vertical perturbations of flow velocity, red lines show pressure perturbations at plus/minus 100, 150, 200, 250, 300 Pa (negative contours are dashed). Hours in UTC are in the upper-left corners, capital letters on top of the plates indicate start and end points of the cross-sections shown in Fig. 22.

The development of RIJ can be better assessed with Fig. 23 that shows vertical cross-sections of wind perturbations through the developing convective cluster. The flow perturbations are calculated relative to the EM-forecast (running without CI) at the cross-section time and place, and its component is shown along the direction of the reference wind averaged over the cross-section in 700-500 hPa layer (the direction is between 130°-140° and the averaged wind velocity diminishes slowly between 12:00 and 15:00 from 16.3 to 13.7 m s⁻¹). Already at 12:00, an increase of wind speed reaching 4 m s⁻¹ at 5 km altitude is seen behind the convective updraft. At 13:00, a 30-km-long zone of positive wind speed perturbation forms in the low-to-mid troposphere behind the strong updraft with a maximum reaching 15 m s⁻¹ at about 3 km altitude, indicating a formation of the RIJ. It may already contribute to surface gusts as its frontal part is caught in a strong downdraft reaching the near-surface area. At 14:00, the length of RIJ exceeds 50 km and its velocity perturbation reaches 18.5 m s⁻¹ in the frontal part of the system, also at about 3 km altitude, where the pressure perturbation exceeds -250 Pa. The middle part of the RIJ, caught in a strong downdraft reaching the near-surface area, likely contributes to the forecasted strong surface gusts. At 15:00, the RIJ intensifies across its extensive area with maximum velocity perturbations reaching 20 m s⁻¹ but a transfer of its momentum to the near-surface area seems to be weaker. The forecast indicates the formation of strong RIJ already at 13:00, in the very early stage of the system development. Moreover, since that time the RIJ is able to influence the magnitude of the 10-m wind gusts.

9 Summary and conclusions

The paper presents a numerical reconstruction of a rapidly-developing, fast-propagating, severe convective meso-β-scale bow echo system that formed over northeastern Poland on 21 August 2007. The system was weakly forced in the sense of the lack of the omega equation forcing for strong synoptic-scale ascent or nearby frontal surfaces. However, it developed in the vicinity of a local convergence zone as indicated by converging



trajectories in Figs. 15 and S-9. The system produced maximum surface wind gusts of 35 m s^{-1} , and caused significant property damage and 12 fatalities.

As discussed in the Introduction, NWP models are – by design – not able to fully represent the physical and dynamical processes acting across the entire range of spatial and temporal scales to develop organized convection. Indeed, we demonstrate that the operational convective-scale COSMO model with a horizontal grid spacing of 2.2 km used for our study encounters significant problems with numerical reconstruction of the event, even with favorable atmospheric environmental conditions and additional application of shallow convection parameterization. However, an implementation of a near-grid-scale stochastic convection initiation (CI) scheme using temperature perturbations reminiscent of $O(1 \text{ km})$ scale PBL thermals allows the relatively coarse-grid and under-resolving model (see the Introduction) to explicitly reconstruct convective development. With a provision of realistic environmental conditions and the CI mechanism implemented within a 9-member ensemble, the model can reconstruct the timing, place, and severity (maximum gusts exceeding 30 m s^{-1}) of the fast-developing and meso- β -scale convective system.

The model realistically reconstructs the system's cold-pool-driven dynamics organized by strong updrafts at the leading edge of its cold pool. The model is able to develop an RIJ of realistic extent and magnitude in early stages of the convective system evolution. The simulations well respond to the increase of low-to-mid tropospheric winds and vertical shear: the maximum gusts of the ensemble and the system's propagation speed increase while the structure of convective updrafts at the cold pools' leading edge is improved. However, the model notably delays the development of the strongest gusts (by almost an hour) and struggles with the formation of a continuous convective line. In contrast to the observations, simulated convective cells that develop on the cold pool leading edge do not merge sufficiently early and tend to stay as isolated entities. The study demonstrates that, despite these drawbacks, the convective-scale NWP models have a valuable potential in prediction of such severe convective systems that have a high social impact.

The following additional comments may be formulated:

--- The study confirms the important role of $O(1 \text{ km})$ -scale variability of atmospheric flows for the development of convective systems such as the one analyzed here. Because of the limited model resolution (mostly horizontal but also vertical), current convective-scale NWP models cannot represent such a variability, and the problem may be alleviated by perturbation methods like the used here CI scheme.

--- For convective processes, the paradigm of perturbation sizes limited by the model's effective resolution can be replaced by physically justified smaller-in-size perturbations resembling those developing within CBL. An interesting avenue for further research opens here as the work of Peters et al. (2022a; b) suggests that there may still exist a physically based horizontal lower size limit for such perturbations in high-shear environments typical for severe convection.

--- The temperature-only perturbations lead not only to perturbations of MCAPE and MCIN but also to perturbations of low-to-mid tropospheric winds and vertical shear. Those perturbations evolve interacting with ambient flow and form local extrema exceeding those of the ambient flow.

--- Local maxima of the vertical shear play an important role in model representation of deep convection initiation and in further development toward the convection organization, arguably due to the dynamical mechanisms analyzed by Peters et al. (2022a; b).

--- The study demonstrates a potential of stochastic near-grid-scale CI scheme for improving operational convective-scale NWP. That would require substantial further work and the relevant issues include linking the



perturbation properties with the CBL properties and ensuring conservation requirements; e.g., Berner et al. (2017).

690 --- Finally, realistic convective case studies using IC/BC derived from global reanalyzes (like ERA5) may benefit from augmenting them with regional DA using available small- and meso-scale observations, including surface characteristics (e.g., soil properties).

Code and data availability

Codes of COSMO model and relevant pre- and post-processing tools are the intellectual property of the COSMO Consortium and are not publicly available. The Meteosat data are available under the EUMETSAT's Data Policy rules. Initial and boundary conditions are publicly provided by DKRZ (Germany) and contain the Copernicus Climate Change Service Information (ERA-5 reanalysis, 2019) technically processed by the COSMO-CLM Community. The SYNOP and TEMP observations were obtained from the GTS systems of WMO (for Europe) and from the database of Institute of Meteorology and Water Management – National Research Institute (for 700 Poland). The latter are available via the <https://danepubliczne.imgw.pl/> web interface.

Supplement

The supplement was submitted with the manuscript.

Author contributions

MZZ and WWG conceived the study and advised DKM during its execution. DKM designed, programmed and 705 ran model simulations, and drafted the initial version of the manuscript. All three authors were involved in drafting its subsequent versions.

Competing interests

The authors declare that they have no conflict of interest.

Acknowledgments

710 The paper is based on and extends the results of DKM PhD study at Institute of Meteorology and Water Management – National Research Institute. Numerical experiments were carried out using the COSMO model and other software maintained by the COSMO Consortium. Computing resources for the experiments were provided by the Institute. External parameters for numerical simulations were obtained by the WebPEP service that is kindly provided by the COSMO-CLM Community. The figures were prepared using NCL software 715 developed at NCAR.



Financial support

This research was supported by Institute of Meteorology and Water Management – National Research Institute in Poland. NSF National Center for Atmospheric Research is sponsored by the NSF under Cooperative Agreement 1852977.

720 References

- Anthes, R. A.: Data assimilation and initialization of hurricane prediction model, *J. Atmos. Sci.*, 31, 702–719, doi:10.1175/1520-0469(1974)031<0702:DAAIOH>2.0.CO;2, 1974.
- Anthes, R. A., Kuo Y.-H., Baumhefner D. P., Errico R. M., and Bettge T. W.: Predictability of mesoscale atmospheric motions, *Advances in Geophysics*, Academic Press, Vol. 28B, 159–202, doi:10.1016/S0065-2687(08)60188-0, 1985.
- Asensio, H., Messmerand, M., Lüthi, D., and Osterried, K.: External parameters for numerical weather prediction and climate application EXTPAR V.5_0: User and implementation guide, Consortium for Small-Scale Modeling, 45 pp., http://www.cosmomodel.org/content/support/software/ethz/EXTPAR_user_and_implementation_manual_202003.pdf, 2020.
- Bach, L., Schraff, C., Keller, J. D., and Hense, A.: Towards a probabilistic regional reanalysis system for Europe: evaluation of precipitation from experiments, *Tellus*, 68A, 32209, doi:10.3402/tellusa.v68.32209, 2016.
- Baldauf, M., Seifert, A., Förstner, J., Majewski, D., Raschendorfer, M., and Reinhardt, T.: Operational convective-scale numerical weather prediction with the COSMO model: description and sensitivities, *Mon. Wea. Rev.*, 139, 3887–3905, doi:10.1175/MWR-D-10-05013.1, 2011.
- Berner, J., and Coauthors: Stochastic parameterization: toward new view of weather and climate models, *Bull. Am. Meteorol. Soc.*, 98, 565–587, doi:10.1175/BAMS-D-15-00268.1, 2017.
- Bouttier, F., Vie, B., Nuissier, O., and Raynaud, L.: Impact of stochastic physics in a convection-permitting ensemble, *Mon. Wea. Rev.*, 140, 3706–3721, doi:10.1175/MWR-D-12-00031.1, 2012.
- 740 Brasseur, O.: Development and application of a physical approach to estimating wind gusts, *Mon. Wea. Rev.*, 129, 5–25, doi:10.1175/1520-0493(2001)129<0005:DAAOAP>2.0.CO;2, 2001.
- Bryan, G. H., Wyngaard, J. C., and Fritsch, J. M.: Resolution requirements for the simulation of deep moist convection, *Mon. Wea. Rev.*, 131, 2394–2416, doi:10.1175/1520-0493(2003)131%3C2394:RRFTSO%3E2.0.CO;2, 2003.
- 745 Bryan, G. H., Kniviel, J. C., and Parker, M. D.: A multimodel assessment of RKW theory’s relevance to squall-line characteristics, *Mon. Wea. Rev.*, 134, 2772–2792, doi:10.1175/MWR3226.1, 2006.
- Bučánek, A. and R. Brožková, R.: Background error covariances for a BlendVar assimilation system, *Tellus*, 69A, doi:10.1080/16000870.2017.1355718, 2017.
- Buizza, R., Miller, M., and Palmer, T.: Stochastic representation of model uncertainties in the ECMWF ensemble prediction system, *Quart. J. Roy. Meteor. Soc.*, 125, 2887–2908, doi:10.1002/qj.49712556006, 1999.
- 750 Celiński-Mysław, D., and Palarz, A.: The occurrence of convective systems with a bow echo in warm season in Poland., *Atmos. Res.*, 193, 26–35, doi:10.1016/j.atmosres.2017.04.015, 2017.



- Celiński-Mysław, D., Palarz, A., and Łoboda, Ł.: Kinematic and thermodynamic conditions related to convective systems with a bow echo in Poland, *Theor. Appl. Climatol.*, 137, 2109–2123, doi:10.1007/s00704-018-2728-6, 2018.
- Chen, Z., Qie, X., Liu, D., and Xiong, Y.: Lightning data assimilation with comprehensively nudging water contents at cloud-resolving scale using WRF model, *Atmos. Res.*, 221, 72–87, doi:10.1016/j.atmosres.2019.02.001, 2018.
- Clark, A. J., and Coauthors: Probabilistic precipitation forecast skill as a function of ensemble size and spatial scale in a convection-allowing ensemble, *Mon. Wea. Rev.*, 139, 1410–1418, doi:10.1175/2010MWR3624.1, 2011.
- Clark, P. A., Roberts, N. M., Lean, H. W., Ballard, S. P., and Charlton-Perez, C.: Convection-permitting models: a step-change in rainfall forecasting, *Meteorological Applications*, 23, 165–181, doi:10.1002/met.1538, 2016.
- Clark, P. A., Halliwell, C. E., and Flack, D. L. A.: A physically based stochastic boundary layer perturbation scheme. Part I: Formulation and evaluation in a convection-permitting model, *J. Atmos. Sci.*, 78, 727–746, doi:10.1175/JAS-D-19-0291.1, 2021.
- Coniglio, M., Weiss, S., Evans, J., Bright, D., Hart, J., Bothwell, P., Corfidi, S., and Johns, B.: NOAA Hazardous Weather Testbed, NOAA Rep., 11 pp., www.nssl.noaa.gov/users/mcon/public_html/2005_summer_exp_plan.pdf, 2005.
- Corfidi, S. F., Coniglio, M. C., Cohen, A. E., and Mead, C. M.: A proposed revision to the definition of “derecho”, *Bull. Amer. Meteor. Soc.*, 97, 935–949, doi:10.1175/BAMS-D-14-00254.1, 2016.
- Cressman, G. P.: An operational objective analysis system, *Mon. Wea. Rev.*, 87, 367–374, doi:10.1175/15200493(1959)087%3C0367:AOOAS%3E2.0.CO;2, 1959.
- Davis, C., and Coauthors: The Bow Echo and MCV Experiment: observations and opportunities, *Bull. Amer. Meteor. Soc.*, 85, 1075–1093, doi:10.1175/BAMS-85-8-1075, 2004.
- Davies, H. C., and Turner, R. E.: Updating prediction models by dynamical relaxation: An examination of the technique, *Quart. J. Roy. Meteor. Soc.*, 103, 225–245, doi:10.1002/qj.49710343602, 1977.
- Dixit, V., Nuijens, L., and Helfer, K. C.: Counter-gradient momentum transport through subtropical shallow convection in ICON-LEM simulations, *J. Adv. Model. Earth Syst.*, 13, e2020MS002352, doi:10.1029/2020MS002352, 2021.
- Doms, G., and Coauthors: A description of the nonhydrostatic regional COSMO-model: Part II: Physical parameterizations, Consortium for Small-Scale Modeling, 167 pp., doi:10.5676/DWD_pub/nwv/cosmo-doc_6.00_II, 2021.
- Done, J., Davis, C. A., and Weisman, M.: The next generation of NWP: explicit forecasts of convection using the weather research and forecasting (WRF) model, *Atmos. Sci. Lett.*, 5, 110–117, doi:10.1002/asl.72, 2004.
- ESA GlobCover 2009 Project: Global Land Cover Map, ESA and UC Louvain, accessed 2 March 2023, http://due.esrin.esa.int/page_globcover.php, 2010.
- FAO/IIASA/ISRIC/ISS-CAS/JRC: Harmonized World Soil Database (version 1.2), FAO and IIASA, accessed 2 March 2023, www.fao.org/soils-portal/soil-survey/soil-maps-and-databases/harmonized-world-soil-database-v12/en/, 2012.
- Figurski M. J., Nykiel, G., Jaczewski, A., Baldysz, Z., and Wdowikowski, M.: The impact of initial and boundary conditions on severe weather event simulations using a high-resolution WRF model. Case study of the



- derecho event in Poland on 11 August 2017, *Meteorology Hydrology and Water Management*, 10, 60–86, doi:10.26491/mhwm/143877, 2021.
- 795 Fujita, T. T.: Manual of downburst identification for project Nimrod, Satellite and Mesometeorology Research Paper 156, Dept. of Geophysical Sciences, University of Chicago, 104 pp., 1978.
- Gallus, W. A., Snook, N. A., and Johnson, E. V.: Spring and summer severe weather reports over the Midwest as a function of convective mode: A preliminary study, *Wea. Forecasting*, 23, 101–113, doi:10.1175/2007WAF2006120.1, 2008.
- 800 Gebhardt, C., Theis, S. E., Krahe, P., and Renner, V.: Experimental ensemble forecasts of precipitation based on a convection-resolving model, *Atmos. Sci. Lett.*, 9, 67–72, doi:10.1002/asl.177, 2008.
- Gerken, T., Babel, W., Herzog, M., Fuchs, K., Sun, F., Ma, Y., Foken, T., and Graf, H.-F.: High-resolution modelling of interactions between soil moisture and convective development in a mountain enclosed Tibetan Basin, *Hydrol. Earth Syst. Sci.*, 19, 4023–4040, doi:10.5194/hess-19-4023-2015, 2015.
- 805 Grabowski, W. W.: Daytime convective development over land: The role of surface forcing, *Quart. J. Roy. Meteor. Soc.*, 149, 2800–2819, doi:10.1002/qj.4532, 2023.
- Grabowski, W. W., and Smolarkiewicz, P. K.: CRCP: A cloud resolving convection parameterization for modeling the tropical convective atmosphere, *Physica D*, 133, 171–178, doi:10.1016/S0167-2789(99)00104-9, 1999.
- 810 Grabowski, W. W., and Coauthors: Daytime convective development over land: A model intercomparison based on LBA observations, *Quart. J. Roy. Meteor. Soc.*, 132, 317–344, doi:10.1256/qj.04.147, 2006.
- Grunzke, C. T., and Evans, C.: Predictability and dynamics of warm-core mesoscale vortex formation with the 8 May 2009 “Super Derecho” event, *Mon. Wea. Rev.*, 145, 811–832, doi:10.1175/MWR-D-16-0217.1, 2017.
- Gustafsson, N., and Coauthors: Survey of data assimilation methods for convective-scale numerical weather prediction at operational centres, *Quart. J. Roy. Meteor. Soc.*, 144, 1218–1256, doi:10.1002/qj.3179, 2018.
- 815 Hacker, J. P., and Coauthors: The U.S. Air Force Weather Agency’s mesoscale ensemble: Scientific description and performance results, *Tellus*, 63A, 625–641, doi:10.1111/j.1600-0870.2010.00497.x, 2011.
- Harrop, B. E., Lu, J., Leung, L. R., Lau, W. K. M., Kim, K.-M., Medeiros, B., Soden, B. J., Vecchi, G. A., Zhang, B., and Singh, B.: An overview of cloud–radiation denial experiments for the Energy Exascale Earth
- 820 System Model version 1, *Geosci. Model Dev.*, 17, 3111–3135, doi:10.5194/gmd-17-3111-2024, 2024.
- Heise, W., Lange, M., Ritter, B., and Schrodin, R.: Improvement and validation of the multi-layer soil model, *COSMO Newsletter*, 3, 198–203, 2003.
- Hersbach, H., and Coauthors: The ERA5 global reanalysis, *Quart. J. Roy. Meteor. Soc.*, 146, 1999–2049, doi:10.1002/qj.3803, 2020.
- 825 Hirt, M., Rasp, S., Blahak, U., and Craig, G. C.: Stochastic parameterization of processes leading to convective initiation in kilometer-scale models, *Mon. Wea. Rev.*, 147, 3917–3934, doi:10.1175/MWR-D-19-0060.1, 2019.
- Holton, J. R.: An introduction to dynamic meteorology, Elsevier Academic Press, pp. 535, 2004.
- Johns, R. H., and Hirt, W. D.: Derechos: widespread convectively induced windstorms, *Wea. Forecasting*, 2, 32–49, doi:10.1175/1520-0434(1987)002<0032:DWCIW>2.0.CO;2, 1987.
- 830 Kienast-Sjögren, E., Miltenberger, A. K., Luo, B. P., and Peter, T.: Sensitivities of Lagrangian modelling of mid-latitude cirrus clouds to trajectory data quality, *Atmos. Chem. Phys.*, 15, 7429–7447, doi:10.5194/acp-15-7429-2015, 2015.



- Klimowski, B. A., Bunkers, M. J., Hjelmfelt, M. R., and Covert, J. N.: Severe convective windstorms over the Northern High Plains of the United States, *Wea. Forecasting*, 18, 502–519, doi:10.1175/1520-0434(2003)18<502:SCWOTN>2.0.CO;2, 2003.
- Klimowski, B. A., Hjelmfelt, M. R., and Bunkres, M. J.: Radar observation of the early evolution of bow echoes, *Wea. Forecasting*, 19, 727–734, doi:10.1175/1520-0434(2004)019<0727:ROOTEE>2.0.CO;2, 2004.
- Kober, K., and Craig, G. C.: Physically based stochastic perturbations (PSP) in the boundary layer to represent uncertainty in convective initiation, *J. Atmos. Sci.*, 73, 2893–2911, doi:10.1175/JAS-D-15-0144.1, 2016.
- Kolonko M., Szczęch-Gajewska, M., Bochenek, B., Stachura, G., and Sekuła, P.: Using ALARO and AROME numerical weather prediction models for the derecho case on 11 August 2017, *Meteorology Hydrology and Water Management*, 10, 88–105, doi:10.26491/mhwm/156260, 2023.
- Kühnlein, C., Keil, C., Craig, G. C., and Gebhardt, C.: The impact of downscaled initial condition perturbations on convective-scale ensemble forecasts of precipitation, *Quart. J. Roy. Meteor. Soc.*, 140, 1552–1562, doi:10.1002/qj.2238, 2014.
- Lawson, J., and Gallus Jr., W. A.: On contrasting ensemble simulations of two great plains bow echoes, *Wea. Forecasting*, 31, 787–810, doi:10.1175/WAF-D-15-0060.1, 2016.
- Lawson, J. R., Gallus Jr., W. A., and Potvin, C. K.: Sensitivity of a bowing mesoscale convective system to horizontal grid spacing in a convection-allowing ensemble, *Atmosphere*, 11, 384, doi:10.3390/atmos11040384, 2020.
- Lebo, Z. J., and Morrison, H.: Effects of horizontal and vertical grid spacing on mixing in simulated squall lines and implications for convective strength and structure, *Mon. Wea. Rev.*, 143, 4355–4375, doi:10.1175/MWR-D-15-0154.1, 2015.
- Liu, W., Ullrich, P. A., Li, J., Zarzycki, C., Caldwell, P. M., Leung, L. R., and Qian, Y.: The June 2012 North American Derecho: A testbed for evaluating regional and global climate modeling systems at cloud-resolving scales, *J. Adv. in Model. Earth Syst.*, 15(4), doi:10.1029/2022MS003358, 2023.
- LeMone, M. A.: Momentum transport by a line of cumulonimbus, *J. Atmos. Sci.*, 40, 1815–1834, doi:10.1175/1520-0469(1983)040<1815:MTBALO>2.0.CO;2, 1983.
- Lorenz, E. N.: The predictability of a flow which possesses many scales of motion, *Tellus*, 21, 289–307, doi:10.1111/j.2153-3490.1969.tb00444.x, 1969.
- Mahoney, K. M., Lackmann, G. M., and Parker, M. D.: The role of momentum transport in the motion of a quasi-idealized mesoscale convective system, *Mon. Wea. Rev.*, 137, 3316–3338, doi:10.1175/2009MWR2895.1, 2009.
- Marquis, J. N., Varble, A. C., Robinson, P., Nelson, T. C., and Friedrich, K.: Low-level mesoscale and cloud-scale interactions promoting deep convection initiation, *Mon. Wea. Rev.*, 149, 2473–2495, doi:10.1175/MWR-D-20-0391.1, 2021.
- Mathias, L., Ermert, V., Kelemen, F., Ludwig, P., and Pinto, J.: Synoptic analysis and hindcast of an intense bow echo in Western Europe: The 09 June 2014 storm, *Wea. Forecasting*, 32, 1121–1141, doi:10.1175/WAF-D-16-0192.1, 2017.
- Mazur, A., and Duniec, G.: Influence of computational grid resolution on the quality of forecasts of dangerous convection phenomena: a case study of August 11, 2017, *Meteorology Hydrology and Water Management*, 10, 106–114, doi:10.26491/mhwm/159068, 2023.



- McGinley, J.: Nowcasting mesoscale phenomena, in *Mesoscale Meteorology and Forecasting*, P. S. Ray, Ed., American Meteorological Society, Boston, 657–688, 1986.
- 875 Mellor, G. L., and Yamada, T.: Development of a turbulence closure model for geophysical fluid problems, *Reviews of Geophysics and Space Physics*, 20, 851–875, doi:10.1029/RG020i004p00851, 1982.
- Melhauser, Ch., and Zhang, F.: Practical and intrinsic predictability of severe and convective weather at the mesoscales, *J. Atmos. Sci.*, 69, 3350–3371, doi:10.1175/JAS-D-11-0315.1, 2012.
- Müller, M., and Coauthors: AROME-MetCoOp: A Nordic convective-scale operational weather prediction
880 model, *Wea. Forecasting*, 32, 609–627, doi:10.1175/WAF-D-16-0099.1, 2017.
- NASA/METI/AIST/Japan Spacesystems and U.S./Japan ASTER Science Team: ASTER Global Digital Elevation Model V003, NASA EOSDIS Land Processes DAAC, accessed 2 March 2023, doi:10.5067/ASTER/ASTGTM.003, 2019.
- Orlanski, I.: A rational subdivision of scales for atmospheric processes, *Bull. Amer. Meteor. Soc.*, 56, 527–530,
885 doi:10.1175/1520-0477-56.5.527, 1975.
- Pacey, G. P., Schultz, D. M., and Garcia-Carreras, L.: Severe convective windstorms in Europe: Climatology, preconvective environments, and convective mode, *Wea. Forecasting*, 36, 237–252, doi:10.1175/WAF-D-20-0075.1, 2021.
- Palmer, T. N.: The ECMWF Ensemble Prediction System: Looking back (more than) 25 years and projecting
890 forward 25 years, *Quart. J. Roy. Meteor. Soc.*, 145, 12–24, doi:10.1002/qj.3383, 2019.
- Palmer, T. N., Döring, A., and Seregin, G.: The real butterfly effect, *Nonlinearity*, 27, R123, doi:10.1088/0951-7715/27/9/R123, 2014.
- Parker, M. D., Borchardt, B. S., Miller, R. L., and Ziegler, C. L.: Simulated evolution and severe wind production by the 25–26 June 2015 nocturnal MCS from PECAN, *Mon. Wea. Rev.*, 148, 183–209,
895 doi:10.1175/MWR-D-19-0072.1, 2020.
- Peters, J. M., Morrison, H., Nelson, T. C., Marquis, J. N., Mulholland, J. P., and Nowotarski, C. J.: The influence of shear on deep convection initiation. Part I: Theory, *J. Atmos. Sci.*, 79, 1669–1690, doi:10.1175/JAS-D-21-0145.1, 2022a.
- Peters, J. M., Morrison, H., Nelson, T. C., Marquis, J. N., Mulholland, J. P., and Nowotarski, C. J.: The influence
900 of shear on deep convection initiation. Part II: Simulations, *J. Atmos. Sci.*, 79, 1691–1711, doi:10.1175/JAS-D-21-0144.1, 2022b.
- Przybylinski, R. W.: The bow echo: Observations, numerical simulations, and severe weather detection methods, *Wea. Forecasting*, 10, 203–218, doi:10.1175/1520-0434(1995)010<0203:TBEONS>2.0.CO;2, 1995.
- Puh, M., Keil, C., Gebhardt, C., Marsigli, C., Hirt, M., Jakub, F., and Craig, G. C.: Physically based stochastic
905 perturbations improve a high-resolution forecast of convection, *Quart. J. Roy. Meteor. Soc.*, 149, 3582–3592, doi:10.1002/qj.4574, 2023.
- Raschendorfer, M.: The new turbulence parameterization of LM, COSMO Newsletter, 1, 89–98, http://www.cosmo-model.org/content/model/documentation/newsLetters/newsLetter01/newsLetter_01.pdf, 2001.
- 910 Reinhardt, T., and Seifert, A.: A three-category ice scheme for LMK, COSMO Newsletter, 6, 115–120, http://www.cosmo-model.org/content/model/documentation/newsLetters/newsLetter06/newsLetter_06.pdf, 2006.



- Ribeiro, B. Z., Weiss, S. J., and Bosart, L. F.: An analysis of the 3 May 2020 low-predictability derecho using a convection-allowing MPAS Ensemble, *Wea. Forecasting*, 37, 219–239, doi:10.1175/WAF-D-21-0092.1, 2022.
- 915 Ritter, B., and Geleyn, J. F.: A comprehensive radiation scheme for numerical weather prediction models with potential applications in climate simulations, *Mon. Wea. Rev.*, 120, 303–325, doi:10.1175/1520-0493(1992)120%3C0303:ACRSFN%3E2.0.CO;2, 1992.
- Rotunno, R., Klemp, J. B., and Weisman, M. L.: A theory for strong, long-lived squall lines, *J. Atmos. Sci.*, 45, 463–485, doi:10.1175/1520-0469(1988)045<0463:ATFSL>2.0.CO;2, 1988.
- 920 Saito, K.: The JMA nonhydrostatic model and its applications to operation and research, *Atmospheric Model Applications*, I. Yucel, Ed., IntechOpen, 85–110, doi:10.5772/35368, 2012.
- Sass, B. H., Petersen, C.: Short range atmospheric forecasts using a nudging procedure to combine analyses of cloud and precipitation with a numerical forecast model, DMI Scientific Report No. 02-01, Danish Meteorological Institute: Copenhagen, Denmark, accessed 6 December 2023,
- 925 <http://www.dmi.dk/fileadmin/Rapporter/SR/sr02-01.pdf>, 2002.
- Schaaf, C., and Wang, Z.: MCD43A1 MODIS/Terra+Aqua BRDF/Albedo Model Parameters Daily L3 Global - 500m V006, NASA EOSDIS Land Processes DAAC, accessed 2 March 2023, doi:10.5067/MODIS/MCD43A1.006, 2015.
- Schättler, U., and Blahak, U.: A description of the nonhydrostatic regional COSMO-model: Part V: Initial and
- 930 boundary data for the COSMO-Model, Consortium for Small-Scale Modelling, 78 pp., doi:10.5676/DWD_pub/nwv/cosmo-doc_6.00_V, 2021.
- Schlemmer, L., Bechtold, P., Sandu, I., and Ahlgrimm, M.: Uncertainties related to the representation of momentum transport in shallow convection, *J. Adv. Model. Earth Syst.*, 9, 1269–1291, doi:10.1002/2017MS000915, 2017.
- 935 Schraff, C.: Mesoscale data assimilation and prediction of low stratus in the Alpine region, *Meteor. Atmos. Phys.*, 64, 21–50, doi:10.1007/BF01044128, 1997.
- Schraff, C., and Hess, R.: A description of the nonhydrostatic regional COSMO-model: Part III: Data assimilation, Consortium for Small-Scale Modeling, 96 pp., doi:10.5676/DWD_pub/nwv/cosmo-doc_6.00_III, 2021.
- 940 Shutts, G.: A kinetic energy backscatter algorithm for use in ensemble prediction systems, *Quart. J. Roy. Meteor. Soc.*, 131, 3079–3102, doi:10.1256/qj.04.106, 2005.
- Skamarock, W. C.: Evaluating mesoscale NWP models using kinetic energy spectra, *Mon. Wea. Rev.*, 132, 3019–3032, doi:10.1175/MWR2830.1, 2004.
- Smull, B. F., and Houze Jr., R. A.: Rear inflow in squall lines with trailing stratiform precipitation, *Mon. Wea.*
- 945 *Rev.*, 115, 2869–2889, doi:10.1175/1520-0493(1987)115<2869:RIISLW>2.0.CO;2, 1987.
- Snively, D. V., and Gallus Jr., W. A.: Prediction of convective morphology in near-cloud-permitting WRF model simulations, *Wea. Forecasting*, 29, 130–149, doi:10.1175/WAF-D-13-00047.1, 2014.
- Sprenger, M., and Wernli, H.: The LAGRANTO Lagrangian analysis tool – version 2.0, *Geosci. Model Dev.*, 8, 2569–2586, doi:10.5194/gmd-8-2569-2015, 2015.
- 950 Stephan, K., Klink, S., and Schraff, C.: Assimilation of radar-derived rain rates into the convective-scale model COSMO-DE at DWD, *Quart. J. Roy. Meteor. Soc.*, 134, 1315–1326, doi:10.1002/qj.269, 2008.
- Surowiecki, A., and Taszarek, M.: A 10-year radar-based climatology of mesoscale convective system archetypes and derechos in Poland, *Mon. Wea. Rev.*, 148, 3471–3488, doi:10.1175/MWR-D-19-0412.1, 2020.



- Tao, W., and Soong, S.: A study of the response of deep tropical clouds to mesoscale processes: three-dimensional numerical experiments, *J. Atmos. Sci.*, 43, 2653–2676, doi:10.1175/1520-0469(1986)043<2653:ASOTRO>2.0.CO;2, 1986.
- Taszarek, M., and Coauthors: Derecho evolving from a mesocyclone - a study of 11 August 2017 severe weather outbreak in Poland: Event analysis and high-resolution simulation, *Mon. Wea. Rev.*, 147, 2283–2306, doi:10.1175/MWR-D-18-0330.1, 2019.
- Tiedtke, M.: A comprehensive mass flux scheme for cumulus parameterization in large-scale models, *Mon. Wea. Rev.*, 117, 1779–1799, doi:10.1175/1520-0493(1989)117%3C1779:ACMFSF%3E2.0.CO;2, 1989.
- Toll, V., Männik, A., Luhamaa, A., and Rõõm, R.: Hindcast experiments of the derecho in Estonia on 08 August, 2010: Modelling derecho with NWP model HARMONIE, *Atmos. Res.*, 158–159, 179–191, doi:10.1016/j.atmosres.2014.10.011, 2015.
- Vallis, G. K.: *Atmospheric and oceanic fluid dynamics*, Cambridge University Press, 769 pp., 2006.
- Varble, A., and Coauthors: Evaluation of cloud-resolving and limited area model intercomparison simulations using TWP-ICE observations: 1. Deep convective updraft properties, *J. Geophys. Res. Atmos.*, 119, 13,891–13,918, doi:10.1002/2013JD021371, 2014a.
- Varble, A., and Coauthors: Evaluation of cloud-resolving and limited area model intercomparison simulations using TWP-ICE observations: 2. Precipitation microphysics, *J. Geophys. Res. Atmos.*, 119, 13,919–13,945, doi:10.1002/2013JD021372, 2014b.
- Varble, A., Morrison, H., and Zipser, E.: Effects of under-resolved convective dynamics on the evolution of a squall line, *Mon. Wea. Rev.*, 148, 289–311, doi:10.1175/MWR-D-19-0187.1, 2020.
- Weisman, M. L.: The role of convectively generated rear-inflow jets in the evolution of long-lived mesoconvective systems, *J. Atmos. Sci.*, 49, 1826–1847, doi:10.1175/1520-0469(1992)049<1826:TROCGR>2.0.CO;2, 1992.
- Weisman, M. L.: The genesis of severe, long-lived bow echoes, *J. Atmos. Sci.*, 50, 645–670, doi:10.1175/1520-0469(1993)050<0645:TGOSLL>2.0.CO;2, 1993.
- Weisman, M. L., and Klemp, J. B.: Characteristics of isolated convective storms, *Mesoscale Meteorology and Forecasting*, P. S. Ray, Ed., Amer. Meteor. Soc., 331–358, 1986.
- Weisman, M. L., Evans, C., and Bosart, L.: The 8 May 2009 Superderecho: Analysis of a real-time explicit convective forecast, *Wea. Forecasting*, 28, 863–892, doi:10.1175/WAF-D-12-00023.1, 2013.
- Wilhelm, J., Wapler, K., Blahak, U., Potthast, R., and M. Kunz, M.: Statistical relevance of meteorological ambient conditions and cell attributes for nowcasting the life cycle of convective storms, *Quart. J. Roy. Meteor. Soc.*, 149, 2252–2280, doi:10.1002/qj.4505, 2023.
- Wójcik, D. K.: Numerical modeling of deep convection: Case study of the 21 August 2007 severe convective system over the Masurian Lake District, Ph.D. thesis, IMGW-PIB, 219 pp, doi:10.5281/zenodo.7700199, 2021.
- Wu, X., and Yanai, M.: Effects of vertical wind shear on the cumulus transport of momentum: Observations and parameterization, *J. Atmos. Sci.*, 51, 1640–1660, doi:10.1175/1520-0469(1994)051<1640:EOVWSO>2.0.CO;2, 1994.
- Wu, X., Grabowski, W. W., and Moncrieff, M. W.: Long-term behavior of cloud systems in TOGA COARE and their interactions with radiative and surface processes. Part I: Two-dimensional modeling study, *J. Atmos. Sci.*, 55, 2693–2714, doi:10.1175/1520-0469(1998)055<2693:LTBOCS>2.0.CO;2, 1998.



- Xu, X., Xue, M., and Wang, Y.: Mesovortices within the 8 May 2009 bow echo over the central United States: Analyses of the characteristics and evolution based on Doppler radar observations and a high-resolution model simulation, *Mon. Wea. Rev.*, 143, 2266–2290, doi:10.1175/MWR-D-14-00234.1, 2015.
- Yamada, H.: Numerical simulations of the role of land surface conditions in the evolution and structure of summertime thunderstorms over a flat highland, *Mon. Wea. Rev.*, 136, 173–188, doi:10.1175/2007MWR2053.1, 2008.
- 1000 Yano, J.-I., and Coauthors: Scientific challenges of convective-scale numerical weather prediction, *Bull. Amer. Meteor. Soc.*, 99, 699–710, doi:10.1175/BAMS-D-17-0125.1, 2018.
- Zeng, Y., Janjić, T., de Lozar, A., Rasp, S., Blahak, U., Seifert, A., and Craig, G. C.: Comparison of methods accounting for subgrid-scale model error in convective-scale data assimilation, *Mon. Wea. Rev.*, 148, 2457–2477, doi:10.1175/MWR-D-19-0064.1, 2020.
- 1005 Ziemiański, M. Z., Grabowski, W. W., and Moncrieff, M. W.: Explicit convection over the western Pacific warm pool in the Community Atmospheric Model, *J. Climate*, 18, 1482–1502, doi:10.1175/JCLI3345.1, 2005.
- Ziemiański, M. Z., Wójcik, D. K., Rosa, B., Piotrowski, Z. P.: Compressible EULAG dynamical core in COSMO: convective-scale Alpine weather forecast, *Mon. Wea. Rev.*, 148, 3563–3583, doi:10.1175/MWR-D-20-0317.1, 2021.